FEA Validation of NiTiPdPt and NiTiPdCu Shape Memory Alloys at High Temperatures

By

Aiman Rashid

NUST201260364MSMME62012F

Supervised by: **Dr. Mushtaq Khan**

Design and Manufacturing Engineering

School of Mechanical & Manufacturing Engineering

National University of Sciences and Technology

Islamabad

August, 2016

FEA Validation of NiTiPdPt and NiTiPdCu Shape Memory Alloys at High Temperatures

By

Aiman Rashid
NUST201260364MSMME62012F

A thesis submitted in partial fulfilment of the requirements for the degree of MS Design and Manufacturing Engineering

Thesis Supervisor:
Dr. Mushtaq Khan

Thesis Supervisor's Signature: _____

Design and Manufacturing Engineering
School of Mechanical & Manufacturing Engineering
National University of Sciences and Technology,
Islamabad
August, 2016

Declaration

I certify that this research work titled "*FEA Validation of NiTiPdPt and NiTiPdCu Shape Memory Alloys at High Temperatures*" is my own work. The work has not been presented elsewhere for assessment. The material that has been used from other sources it has been properly acknowledged / referred.

Signature of Student

Aiman Rashid

NUST201260364MSMME62012F

Plagiarism Certificate (Turnitin Report)

This thesis has been checked for Plagiarism. Turnitin report endorsed by Supervisor is attached.

Aiman Rashid
NUST201260364MSMME62012F

Signature of Supervisor
Dr. Mushtaq Khan

Copyright Statement

- Copyright in text of this thesis rests with the student author. Copies (by any process) either in full, or of extracts, may be made only in accordance with instructions given by the author and lodged in the Library of NUST School of Mechanical & Manufacturing Engineering (SMME). Details may be obtained by the Librarian. This page must form part of any such copies made. Further copies (by any process) may not be made without the permission (in writing) of the author.
- The ownership of any intellectual property rights which may be described in this thesis is vested in NUST School of Mechanical & Manufacturing Engineering, subject to any prior agreement to the contrary, and may not be made available for use by third parties without the written permission of the SMME, which will prescribe the terms and conditions of any such agreement.
- Further information on the conditions under which disclosures and exploitation may take place is available from the Library of NUST School of Mechanical & Manufacturing Engineering, Islamabad.

Acknowledgement

I am thankful to my Creator Allah Subhana-Watala to have guided me throughout this work at every step and for every new thought which You setup in my mind to improve it. Indeed I could have done nothing without Your priceless help and guidance. Whosoever helped me throughout the course of my thesis, whether my parents or any other individual was Your will, so indeed none be worthy of praise but You.

I am profusely thankful to my beloved parents who raised me when I was not capable of walking and continued to support me throughout in every department of my life and my siblings for their guidance, support, care and prayers.

I would also like to express special thanks to my research supervisor Dr. Mushtaq Khan for giving me opportunity, guidance, his kind support and encouragement throughout my thesis and also for the courses which he has taught me. I can safely say that I haven't learned any other subject in such depth than the ones which he has taught.

I would also like to pay special thanks to my Lab fellows and friends especially my senior for support and cooperation. Each time I got stuck in something, he came up with the solution. Without their help I wouldn’t have been able to complete my thesis. I appreciate their patience and guidance throughout the whole thesis.

I would also like to thank Dr. Syed Imran Husain Jaffery, Dr. Shahid Ikramullah Butt, and Dr. Aamir Mubashar for being on my thesis guidance and evaluation committee and express my special thanks to Dr. Liaqat Ali for his help. I am also thankful to everyone at CAD/CAM lab and IT personnel for their support and cooperation.

Finally, I would like to express my gratitude to all the individuals who have rendered valuable assistance to complete this work.

Dedication

I dedicate my efforts to my beloved parents who made me what I am today, my teachers for guiding me all the time consistently, my siblings for backing me up in all thick and thin and my students for inspiring me.

Abstract

Shape Memory Alloy (SMA) also known as smart metal, memory metal, memory alloy, muscle wire, smart alloy is an alloy that "remembers" its original, cold-forged shape: returning to the pre-deformed shape when heated. This material is a lightweight, solid-state alternative to conventional actuators such as hydraulic, pneumatic, and motor based systems.

The Cu-based, Fe-based and NiTi-based SMAs are considered as engineering materials. The yield strength of SMA is lower than that of conventional steel, but higher yield strength than plastic or aluminium. The yield stress for NiTi can reach 500 MPa.

Some devices are made to test the properties of SMA but the research is still in progress to authenticate the experimental results with the true behaviour of SMA. To cope up with this problem, a numerical simulation based solution is needs to be devised to check the thermomechanical properties of newly constituted SMA and verify its load and temperature bearing capacity as well as deformation evaluation.

In this research, one experimentally tested and verified SMA NiTiPdPt is simulated Finite Element Analysis package and the results are compared with the newly constituted SMA NiTiPdCu. The results found for both materials verifies the authenticity and validation of FEA method for evaluation of thermomechanical properties of SMA.

.

Table of Contents

List of Figures

List of Tables

Nomenclature

Symbol	Description	Unit
A	Cross-sectional area	m^2
α	End-condition constant	
C	Spring index	
C_1'	Elastic constant	
C_2'	Elastic constant	
d	Diameter of spring wire	m
D	Mean diameter of spring coil	m
E	Modulus of elasticity	GPa
F	Axial force	N
G	Modulus of rigidity	GPa
J	Mass moment of inertia	m^4
k	Spring rate or scale	$N\ m^{-1}$
K_W	Wahl factor	
K_s	Shear-correction factor	
K_B	Bergsträsser factor	
L_0	Free length of spring	m
λ_{eff}	Effective slenderness ratio	
N	Number of coils	

N_a	Number of active coils	
r	Mean radius of spring coil	m
S_{ut}	Ultimate tensile strength	MPa
S_{sy}	Torsional yield strength	MPa
S_y	Yield strength	MPa
T	Torsional moment	J
τ	Shear stress	Pa
$\tau_{\max}$	Maximum shear stress	Pa
U	Total strain energy	J
y	Deflection	m
y_{cr}	Critical deflection	m

CHAPTER 1

INTRODUCTION

1.1 Significance

There is a number of metallic alloys that have been exhibit the shape memory effect. Wayman gives a comprehensive definition of alloy (SMA) which involves the majority of all the thermal shape memory alloys. He states

> "A thermal shape memory alloy as an article that when deformed at a lower temperature will regain its *original* shape when heated to a higher temperature [1]."

Shape memory alloys are utilized as a part of numerous engineering applications [2]. The most common commercial system is NiTi based SMAs. Applications up to this point for NiTi combinations include electrical switches, micro-actuators, temperature sensitive valves, appliance controllers, cell phones antennas, brassiere underwires, eyeglass frames and countless dental and medical devices [3, 4]. In addition, the first vast scale commercial applications for shape memory alloys were made utilizing NiTi and NiNbTi alloys with sub-rooms changed temperatures, for use as coupling for tubes, funnels, tubes, and electrical interconnects [5]. These applications make utilization of NiTi alloys close room temperature. The fundamental reason that commercial applications have been constrained to close room temperature is that commercial NiTi SMAs have a highest changed temperature of about 100 °C.

Likewise, there are many control and activation-sort applications for materials displaying the shape memory impact at maximum temperatures. Maximum temperature alloys (HTSMA) could be utilized as a part of an aeronautic, power generation [6], chemical processing industries and automotive. While particular applications have been distinguished in light of some type of a HTSMA, no appropriate material have been created. As is normal in the material the improvement of utilizations for cutting edges is somewhat in front of material advancement

itself, and such is the situation for the advancement of high- temperature shape memory compounds.

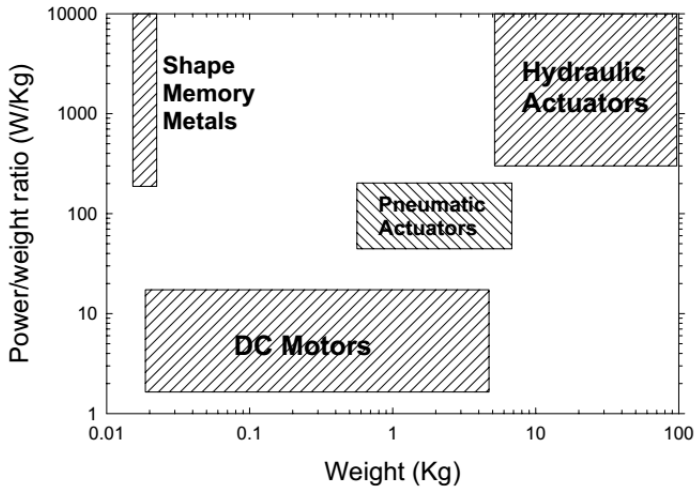

Figure 1.1 Power-to-weight ratio versus weight diagram for common actuator types currently used in aeronautics [6]

Integration of SMA actuators into aeronautic turbomachinery would bring about few natural advantages. Aeronautics plainly stresses weight reduction in all stages of engineering. Decreases in the net weight brings about sizable expansions in fuel effectiveness. Also, SMA actuators diminish the quantity of subsystems when contrasted with standard with typical pneumatic or more common hydraulic and motor-driven actuators, giving additional decreases in weight and cost. Figure 1-1 demonstrates the common weight to power proportions of the more typical commercial actuators now utilized by the aviation industry [7]**.** Limiting weight and expending power brings about an execution file in which SMA actuators are plainly predominant.

The design and development of effectively controlled SMA gadgets requires top to bottom portrayal of the mechanical and shape memory particular properties. Past reviews have been represented compositional impacts of change temperature and, in a few cases, stack free recuperation, yet there is an entire absence of information required for the application of shape memory alloys especially in actuator-related applications. This study endeavors to describe these properties and associate them to material composition and microstructure, which thusly can be utilized to distinguish conceivable ranges for further alloy and process development.

1.2 Background

1.2.1 General Shape and Memory Alloy Behavior

SMAs are categorized by a set of temperatures at which a crystallographic auxiliary change starts and stops. The high-temperature austenite or present stage is a high symmetry stage generally requested while the lower temperature marten site stage is a lower symmetry structure which shapes from the high symmetry present stage diffusion-less shear change. The different temperature at which this change starts and closures on warming and cooling the characterized A_s, M_s, A_f and M_f.

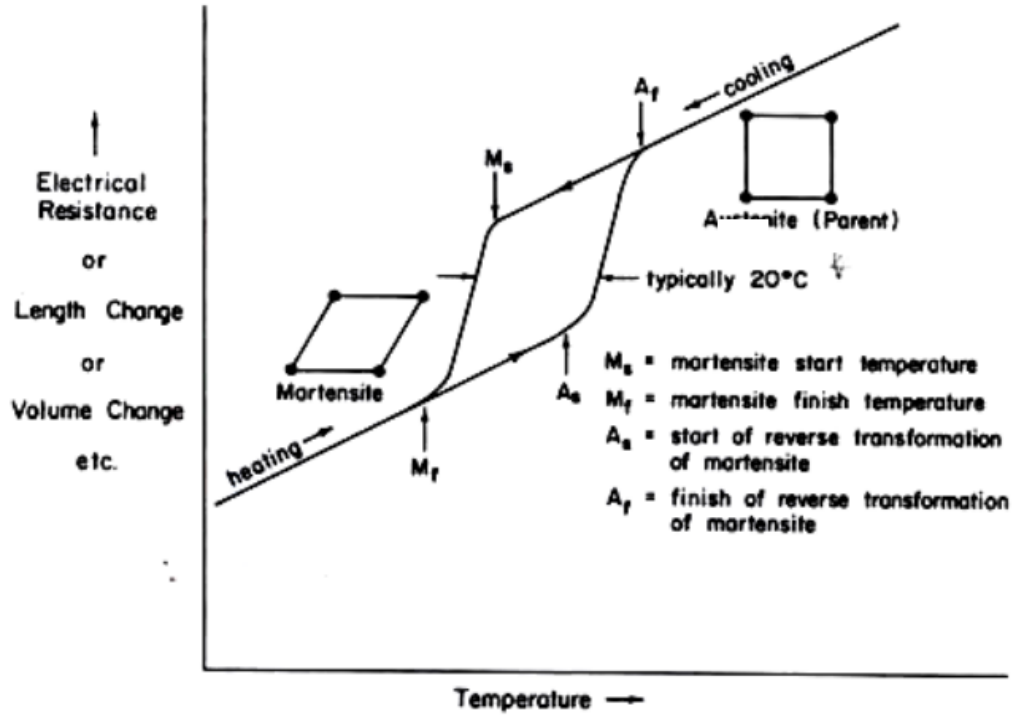

Figure 1.2 Power-to-weight ratio versus weight diagram for common actuator types currently used in aeronautics [8].

The austenite begin temperature, A_s, is the temperature at which the change of the martensite to austenite stage starts on warning. A_f is the temperature at which the change is finished and the material is 100% austenite. The martensite start, M_s and martesite end, M_f, temperatures are the temperatures at which the change happens on cooling [9].

Figure 1.2 is a traditional schematic introduction by Wayman which demonstrate a material property subordinate changes a shape memory alloy is burned through a thermal hysteresis [8].

An Irregularity in the materials properties emerges at the beginning of the change in heating or cooling, which is typical for all SMA materials. All through the change the material properties, this property might be for instance particular volume, electrical resistivity, modulus, or other fundamentally subordinate property. The most widely recognized test strategies for the assurance of the change temperatures are thermal techniques (DSC and DTA) dilatometric strategies, and resistive techniques. The last two outcome in comparable hysteresis plots as exemplified in Figure 1.2. While this figure 4 is glorified it is illustrative of a large number of the significant qualities of thermal shape memory alloys.

1.2.2 SMA Structural Characteristics

Shape memory alloys display both a thermodynamically and crystallographically reversible change. A crystallographically change is probably at the point when the interface between the martensite and austenite is basically cognizant and the parent austenite stage is an ordered compound. The high-temperature austenite stage is a higher-symmetry structure, normally ordered cubic (B2 structure) as in case of NiTi, also, NiTi changed compounds. The austenite stage changes without considerable long range dispersion into a lower symmetry martensite structure at some decrease temperature. Basic cells schematically delineating the structures basic in NiTi higher and lower the change temperatures are appeared in Figure 1.3 [10].

The cubic *B*2 parent stage in NiTi based SMAs changes to various distinctive martensitic structures. The last structure lies on upon alloying additions, polluting influences, and preparing history [7, 9]**.** The following change responses have been distinguished.

$$\left.\begin{array}{l} B2 \leftrightarrow B19 \\ B2 \leftrightarrow B19' \\ B2 \leftrightarrow B19 \leftrightarrow B19' \\ B2 \rightarrow R \rightarrow B19 \end{array}\right\} \qquad (1.1)$$

Every response is crystallography reversible except for the $B2 \rightarrow R$ change. The *R* stage is accomplished by stretching of the *B*2 structure resulting in a rhombohedral structure [10]**.**

The *B*19 stage is an orthorhombic structure which is shaped from the *B*2 parent crystal in a few stages, which comprise of prolongation about the *a*, *b* and *c* axes and shearing of the basal plane in the *c*–direction which is common to the b direction. The *B*19 non-basal plane, which

is typical to the *a*– bearing in the *c*–direction [10]. The *B*19′ stage is the essential shear structure which show up in parallel NiTi leading to the shape memory impact.

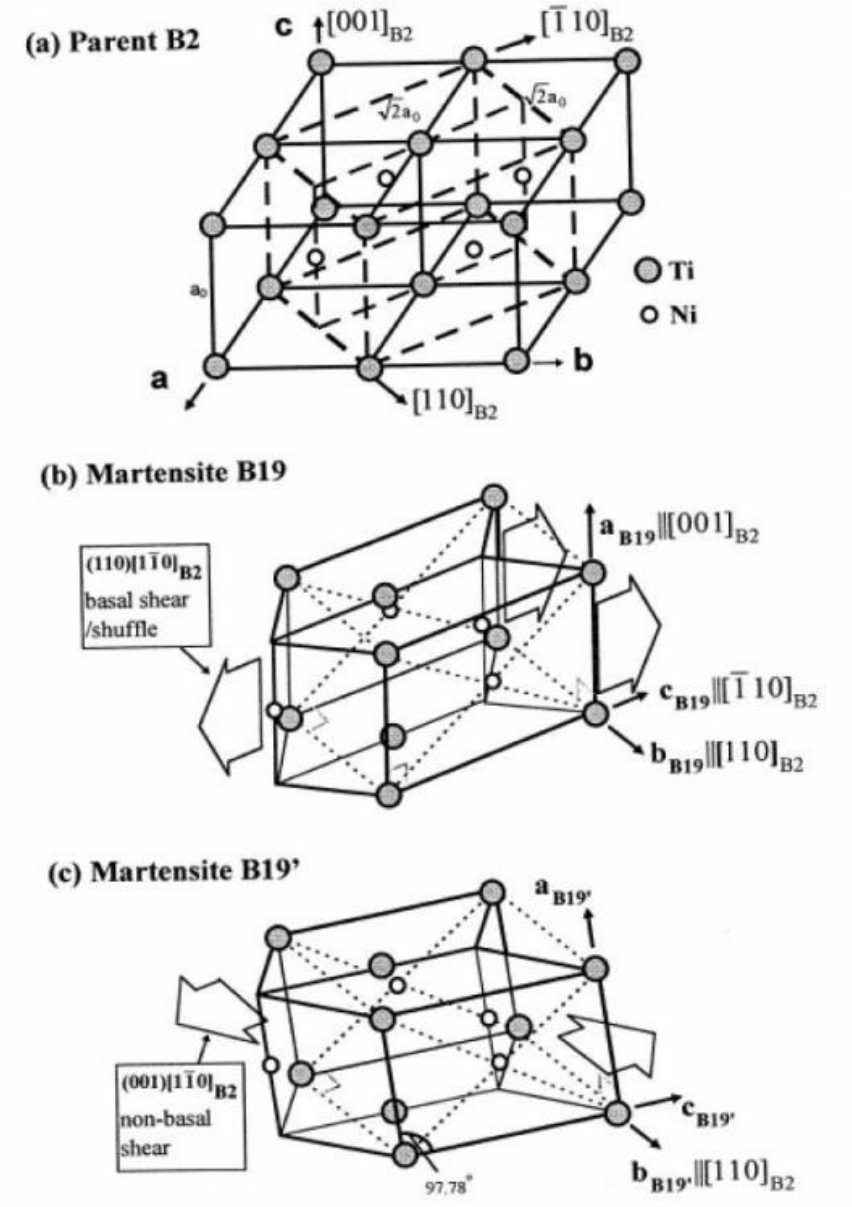

Figure 1.3 Structure of the parent phase (austenite) and shear phases (B19 and B19' martensite) [10].

The cubic parent stage in NiTi SMA is steady at high temperature (over the AF). Numerous lattice variations of martensite can shape from each parent austenite grain. Each variant will take after a superbly reversible way back to the parent austenite stage due to the ordered way of the compound. On the off Chance that this did not happen, the material would experience a diffusional change in the synthetic ordering of the first parent stage's lattice [11].

In the Pt and Pd adjusted NiTi SMAs the *B*19 stage is of essential significance since alloying increases more noteworthy then around 10% outcomes in the essential martensitic structure changing from the monoclinic B19′ to the orthorhombic *B*19 [12]. The *B*19 and *B*19′ are shear structures of the *B*2 and in this way, display a lower symmetry, with the *B*19′ are shear structure of the *B*2 and in this way, display a lower symmetry, with the *B*19′ having the least symmetry [13]. The symmetry of the structure is of significance as it is the fundamental consider the assurance of the quantity of identical martensitic variations which may frame from a parent *B*2 cubic structure. The *B*19 has 12 proportional variations that may frame from a parent crystal. This means 12 distinctive approaches to shear the *B*2 structure in the development of the *B*19. Every identical B19 structure may then bearing to shape a *B*19′ martensite which brings about 24 comparable variants [14]. By and large when breaking down shear structures the quantity of proportionate variations increments as the symmetry of the shear structures the quantity of proportionate variations increments as the symmetry of the shear structure diminishes. This relationship will be analyzed in further detail as it identifies with the disfigurement behavior and mechanisms in the shape memory alloy covered in this study.

The primary theory of martensite development, which applies to both thermoplastic and thermoelastic changes, relays a high symmetry parent structure to a variation of the shear structure. Despite the fact that this theory is appropriate to many shear stage changes for graphic purposes that will concentrate in the structures appeared in Figure 1.3. Three key disfigurements steps are essential to identify with structures by an absolutely shear transformation [15].

1. Primarily there is a Bain distortion which achieves its name generally from the distortion seen in the thermoplastic change which shapes the metastable tetragonal martensite. The Bain distortion is basically the lengthening of the parent stage which is appeared in Figure 1.3 as the extensions of the *a*, *b* and *c* axes.

2. Secondly a shear distortion must happen so as to safeguard the grid symmetry which joined with the Bain distortion frames the undistorted plane or propensity plane.

3. At long last there is a pivot which brings the undistorted plane into a similar orientation in both the parent and shear stage.

The accommodation of random shearing of the lattice (noted as step 2) is a key component characterizing whether a shear change is thermoplastic or themoelastic. Thermoplastic

changes, for example, those moral in steels are non-reversible and the greater part of the change shear related with step 2 is accommodated plastically. That is, there is the development of non-reversible imperfections, for example separation movements and generation. Thermoelastic changes then again accommodate the greater part of the change shear flexibly in mix with recoverable mechanisms.

There are three fundamental ways the change shear might be suited, two of which are adjustable. The dynamic shear component depends to a limited extent on the mechanical properties of the austenite and martensite including the magnitude of the change shear. In both thermoelastic and thermoplastic changes a lot of shear is accommodated flexibly which is dependent to the yield quality of the martensite and austenite nearby the interface [16]. If the change strain brings about an interface stretch state which surpasses its nearby yield quality change strains are suited irreversibly by plastic distortion or slip. At long last, if the shear stress at the interface required to start disfigurement twins is adequately low and higher than the yield quality the change strain is suited by twin formation [17].

Twin accommodated strain, which is the foundation of shape memory alloy, forms during the change along the twin planes in the shear (martensite) stage. It is critical to note that the twinning plane is generally a low index plane that is not parallel to the habit plane. Figure 1.3 is a schematic of the way of a thermoelastic change interface amongst parent and shear stages in which the change strain is accommodated by twin arrangement. The microscopic visible shear plane, which isolates the cubic and shear structures is subject to the auxiliary connections between the martensite and austenite which incorporate Bain shear and pivot [18]. The twinning plane however depends on the symmetry of the shear structure as the deformation twin must just reorient the structure by an associated development of molecules consistently conveyed over the volume isolated by the twinning plane. The change shear along the plainly visible shear plan is in part accommodated by the shear related with twinning along the twin planes [19]. In thermoelastic changes the net changes shear in the martensite is suited to some degree by the versatile deformation of the twinned and untwined locales and incompletely by the formation of the deformation twins. If the deformation twins did not arise the pressure because of the changes strain would surpass the yield quality of the material and in this manner, be accommodated plastically. Twins that shape through thermoelastic changes, with a specific end goal to accommodate the shear along the plainly visible shear plane, have a twin linked crystallographic relationship to each other [20].

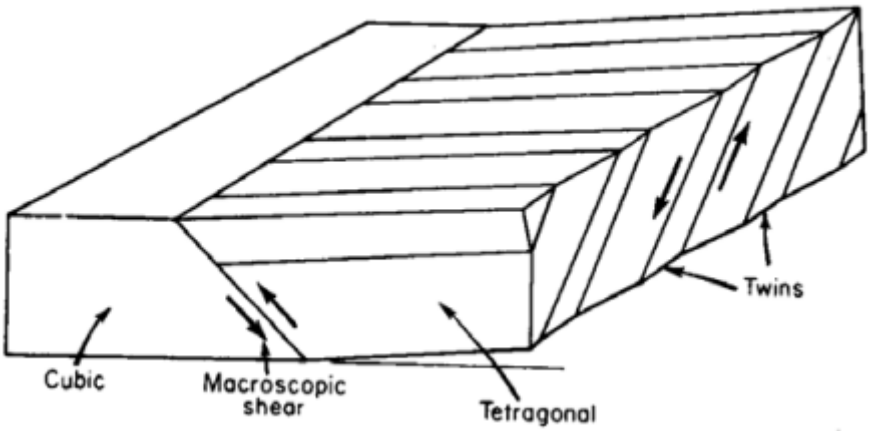

Figure 1.4 Thermoelastic transformation and twin accommodated transformation strain [15].

As exemplified in Figure 1.4 the feeling of the shear related with a twin must substitute between twinned areas. This rule for the settlement of the change strain brings about the arrangement of coupled sets of twinned pairs to in the phenomenological theory of martensite arrangement as reporter variation pairs [21-26].

Although numerous variation sets may shape from an austenite crystal every variation pair is comparable, in this way it is feasible for the austenite to change a single correspondent variation pair which accommodates the change strain by twin formation. This however does not happen in an un-one-sided (no outside pressure) test. What is watched is that austenite changes into a pretty much arbitrary orientation distribution of variant sets. An expansion mechanical imperative must be considered to inspect the driving force for the observed appropriation of variant sets. The fundamental system driving such a circulation comes from the minimization of the microscopic visible state of the bulk material [21].

The change result of the austenite is in various areas of the crystal changes in such a way, to the point that there is no microscopic shape change. This behaviour is stated as self-accommodation. Self-accommodation is a game plan of martensitic variations to such an extent that the sum of their displacements with the boundary suffers no net displacement. It is conceivable to put a self-accommodation arrangement within an austenitic matrix and not persuade any microscopic strains [27]. Self-accommodation is a main property for all themoelastic changes as it limits interface stresses guaranteeing interface coherence and versatile accommodation of strains. In other Words, if self-accommodation did not happen as the interface progresses the pressure in the interface would proceed to rise and rapidly

outperform its yield quality bringing about plastic deformation and lost coherency. Such is the situation in twinned ferritic martensites, where despite that the twinning procedure is reversible, the arrangement of twins in with the end goal that the interface pressures result in plastic deformation and therefore a non-recoverable change.

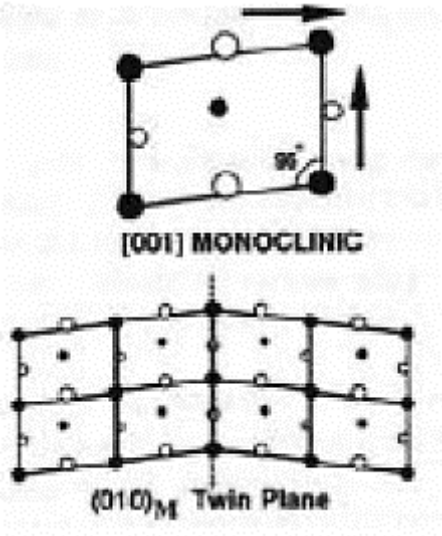

Figure 1.5 Two-dimensional lattice schematic of monoclinic structures [28].

In shape memory alloys the thermoelastic change outcomes in a twinned structure. Figure 1.5 demonstrates a simplified depiction of two equal monoclinic variations isolated by a twin boundary. Although more strain could be suited by the extra interpretation related with the arrangement of an incoherent twin the interfacial energy of a coherent twin boundary is by and large a order of magnitude lower than the energy of an incoherent twin subsequently extra energy is required to shape incoherent twins [22]. Subsequently the arrangement of coherent twin interfaces between martensite variants is thermodynamically positive and extra energy is required to shape incoherent twins.

Figure 1.6 are TEM micrographs of a paired NiTi shape memory alloy [2]. This Figure demonstrates the contrasts between a twinless martensitic structure Figure 1.6**(a)** and a finely twinned structure Figure 1.6**(b)**. Both structures are monoclinic contrasting just by the nearness of a fine distribution of disformation twins that shape during the stage change. The detwinned structure appeared in micrograph Figure 1.6**(a)** resulted because of distortion by detwinning of the martensite. Another crucial part of shape memory alloy is deformation of the martensitic structure through detwinning [29].

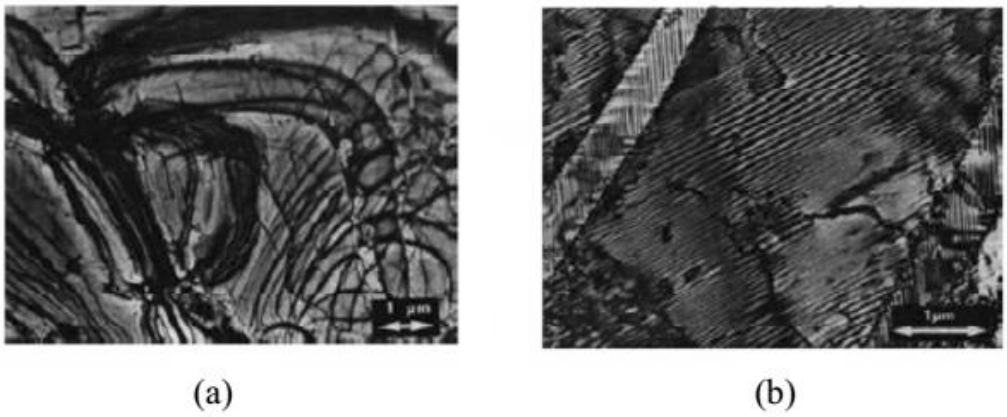

Figure 1.6 TEM micrographs of twinned and untwined monoclinic martensite [28].

An entirely reversible basic change requires that the parent-martensite interface be gissile in the forward and reverse directions. In addition, thermal hysteresis must be small. Ling and Owen have demonstrated that sessile dislocation loops and other defects in the matrix facilitate the movement of the interface [23].

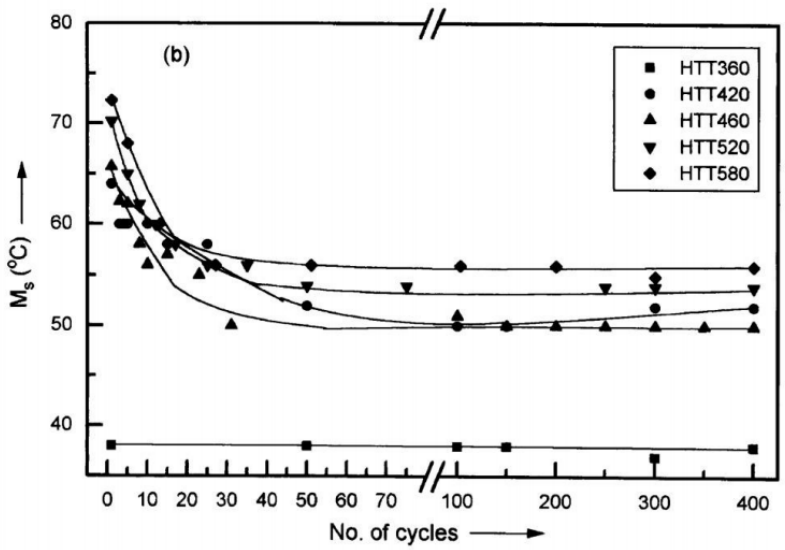

Figure 1.7 Effects of thermal cycling through the hysteresis on the transformation temperatures of several NiTi based shape memory alloys [24].

Moreover these sessile defects increase the plastic flow pressure of the matrix hence making the accommodation of strain by slip more difficult. Mechanically the matrix is adequately fortified and the energy required to move the parent martensite interface is dropped. This has been related to NiTi bases SMAs and additionally other SMA systems. The thickness of these deformities increases with thermal cycling up as far possible resulting in a change temperatures

with expanded thermal cycles. Decreasing change temperatures with thermal cycling has been observed experiement as an appeared in Figure 1.7 [24].

1.2.3 SMA Mechanical Behavior

Metals that show a thermal shape memory impact deform through twin boundary movement. Recoverable deformation of the martensite by twinning responses must happened at pressure lower than those for non-crystallographically reversible responses. Non-crystallographically reversible reaction incorporate dislocation generation and movement. Basically, twins are shaped in the martensite during the forward response isolating comparable variants. Numerous martensite variants arrangements is driven by the minimization of the net transformational stresses [30]. Consequently, twins are available in the microstructure after change; hence, nucleation by a connected shear is not necessary in contrast to standard deformation twinning. Deformation happens by the development of variants most positively lined up with the biggest principle shear part of Schmidt factor at the cost of those with the lowest element. This mechanical is generally referred to as detwinning. Deformation by this system decreases the quantity of twins in the alloys [31]. This is schematically appeared in Figure 1.8. The arrow shows twin planes in the schematic. An allied shear outcomes in the twin boundary movement toward the ordinary path to the shear and the development of a relating variant. Upon completely detwinning the alloy, the material theoretically exists as a solitary variant despite the fact that the degree of detwinning relies upon crystal structure and the related number of proportional variants and additionally the current variants circulation preceding deformation [32].

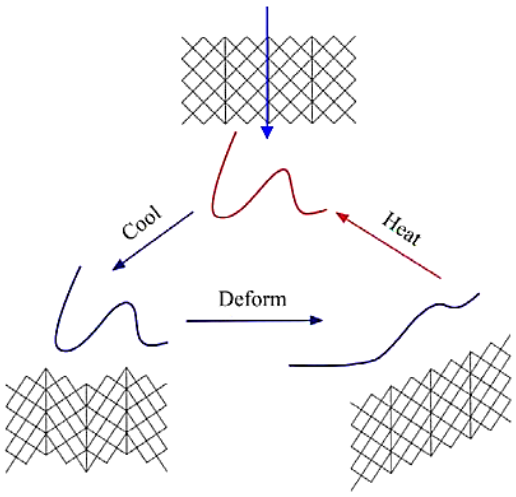

Figure 1.8 Deformation and shape recovery by detwinning (twins marked with arrows) [21].

The distinctive macroscopic mechanical behavior of shape memory alloy is shown in Figure 1.9. This figure is a schematic of the universal pressure strain bends show in these systems below and the M_f temperature. It should be observed that the alloy's composition, thermal and mechanical history may change this curve. It is too conceivable to have different dynamic deformation systems, which will influence the work solidifying rate during the detwinning area of this curve. This figure shows the prefect case for the shape memory effect [33].

The early part of the pressure strain curve is credited to flexible deformation of the unreformed martensite. After achieving basic pressure, detwinning of the martensite starts. The detwinning stress is free of twin thickness and in this way an area in the stretch strain curve exists in which the stress required to twist the material is autonomous of strain [34]. A critical level is come to at the point where positively arranged variants are most pervasive in the microstructure and in this way reactants of the detwinning responses that supply the growth of the positively arranged twins are devoured. At this point twins with comparable Schmidt influence may block on each other. The outcome is an increase in stress-strain relationship that is ascribed to flexibly deforming the detwinned martensite. A moment yield point is apparent at which the critical stress for slip is come to. Non-reversible deformation mechanisms are dynamic in this area therefore the strains are not recoverable by shape memory processes [35].

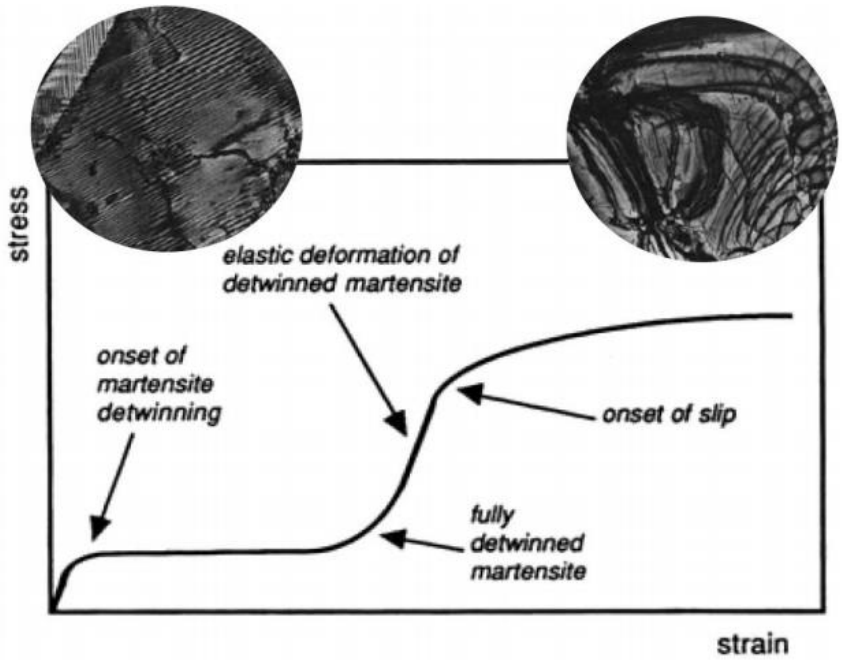

Figure 1.9 Isothermal stress strain behavior of a typical SMA strained in the fully martensitic state [3].

Figure 1.10 is a progression of hypothetical stress-strain curve that graphically show to the three-particular deformation behavior exemplified by SMAs and the temperatures at which they might be active [25]. At temperature over the A_f the Shape memory alloy is austenitic and deformation happens by elastic loading of the austenite taken after by slip. Beneath the M_f temperature the shape memory alloy is completely martensitic and deformation happens by the detwinning systems portrayed previously. SMAs exhibit an unprecedented super elastic impact which happens when the material is deformed over the M_d temperature and under the M_d temperature (Figure 1.10). The M_d temperature is characterized as the temperature at which mechanical stresses can instigate a martensitic change. Ensuing evacuation of the external stress brings about a non-diffusional inversion to the thermodynamically stable parent stage. Versatile strains achievable in NiTi Shape memory alloys are 20X those of carbon spring steels [36].

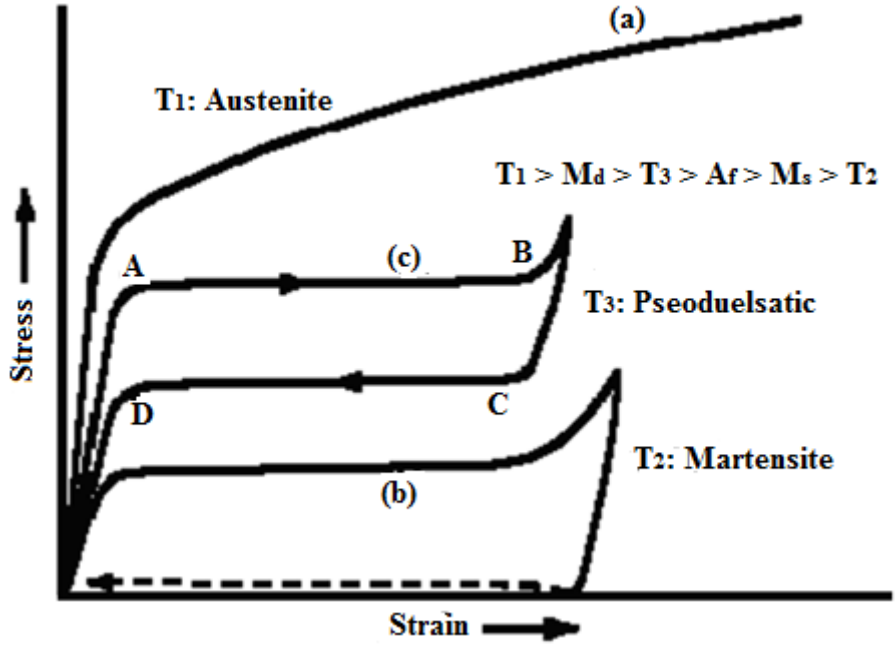

Figure 1.10 Stress strain behavior showing the three main deformation regimes active in SMAs [37].

1.2.4 Thermoelastic Shear Transformations

The thermodynamics of shape memory alloys and the significant shear changes is an unpredictable subject, which includes a composition between the chemical and non-chemical driving force. It is expressed that martensite shapes from the parent stage by an absolutely duffusionless shear change. The change front progresses by shear nuclear movements and the

interface between the martensite and parent stage is lucid [38]. Basically, the martensite brings about a net shape change of every identical variant. As on account of NiTi addressed previously a cubic structure changes to a monoclinic or orthorhombic. This net shape change results in an accommodation strain. The local strain around every variant can be accommodated plastically, flexibly or as a blend of both. This marvel has been assessed and the key thermodynamic parameter distinguished by Reed and Abbaschian [26].

Table 1 was arranged from production [1, 22, 39]. The listed features are basic to SMA systems. The mechanical and structural features already have been expressed. Therefore, as a result of these structural features a particular set of thermodynamic characteristics arises.

Table 1.1: Some features common to metallic thermal SMAs.

Structural features of SMAs [1].
• Ordered parent > ordered martensite • Martensitic change is thermoelastic • Martensite is crystallographically reversible
Thermodynamic features characterized by Dunne and Wayman [40]
• Small chemical driving force at Ms • Small transformational volume and shape change • High flow stress parent matrix
Further mechanical features characterized by Ling and Owen [22]
• Parent –martensite interface must be glassily in both transformation directions • Pre-martensite elastic softening

A key condition for the shape memory effect is that the change must happen reversibly. Accommodation of the transformational strains contiguous the interface could be elastic, plastic, or a blend of both. For the situation where the lion's share the strain is suited flexibly the interface can move in both directions referred to as a thermoelastic change. Thus, the

chemical driving force need to drive the response is small. This is the situation in alloys showing the shape memory effect, which are all the more accurately characterized as thermoelastic changes [41].

In thermoplastic changes, the change strain is suited plastically because of a low flow stress in the parent stage and an extensive transformation strain. For this situation, the changes on the forward and reverse happen at higher chemical driving forces through the nucleated and quick development of the martensite. Normally, individual shear plates are nucleated at imperfections and grow irreversibly [42].

Consequent thermal cycles result in new plates nucleating as opposed to reversible interface movement. A great example of such a situation in the martensitic change of carbon steels where the thermal hysteresis is large and the vast majority of the transformational strains are accommodated plastically [43].

Ortin and planes gracefully treated thermodynamics of thermoelastic effects and systematically characterized conditions for a thermoelastic energy balance. Thermoelastic changes are restricted by the chemical free energy. At equilibrium, it would be predictable that the change happens when the chemical free energy of the parent stage is a minor amount larger than that of shear stage [44]. Though it's not the case that has been shown. In reality, the chemical driving force in thermoelastic change are opposed by non-chemical forces are nearly equal. Following the approach and notation exhibited by Ortin and planes, thermodynamic balance is shown by the following equation.

$$\Delta G_{p..m} = -\Delta G_{ch} + \Delta G_{nch} = 0 \tag{1.2}$$

$G_{p..m}$ is the molar free energy of change, G_{ch} is the molar chemical free energy and G_{nch} is a moral non-chemical energy. At equilibrium, the molar free energy of change is equal to zero therefore the chemical contributions are equal to the non-chemical contribution [45].

The non-chemical contributions comprise of few components, the most conspicuous are the elastic free energy and work done against frictional forces. The frictional and elastic terms comprise of a few parts [46].

The elastic and frictional terms comprise of a numerous part. It was expressed that a condition for thermoelastic change is that most of the transformational strain are accommodated for

elastically. So, there exists an interfacial energy related with the parent martensite interface and aslo the interfaces between variants (twin boundaries) [47].

$$\left.\begin{aligned} \Delta G_{nch} &= \Delta G_{el} + E_{friction} \\ \Delta G_{ch} &= \Delta G_{nch} \\ \Delta G_{ch} &= \Delta G_{el} + E_{friction} \end{aligned}\right\} \tag{1.3}$$

Both contributions are reversible along these lines they have been assembled into the elastic term despite the fact that the interfacial energy is not genuinely an elastic contribution. This is in accordance with the convention set by Ortin and Planes [48].

Frictional energy losses are non-reversible losses primarily because of interface movement. This term might be dealt with as irreversible work done on the system. Three noteworthy parts have been recognized by Olsen and Cohen [37, 49]. These incorporate

1. frictional stresses need to move interfaces

2. irreversible free energy identified to defects made during the change and

3. frictional stresses need to move interface.

It is significant to note that assuming all or the greater part of the accommodation happens plastically the flexible term will be small and the frictional energy losses term will be the primary restricting energy to the chemical driving force. Thus, a huge non-reversible hysteresis will be obvious just like the case in carbon steels as stated before [50].

The fundamental thermodynamics and mechanism which control general conduct of shape memory alloys have been observe. Essentially the structural relationships between the parent in shear stages result in thermomechanical characteristics special to shape memory alloys. Also, driving forces and the relating thermodynamic for thermoelastic changes have been briefly explained and contrasted with thermoplastic changes [51]. A persistent issue that will be explained in consequent chapters brings up that plastic accommodation by non-recoverable procedures hinder the sought-after attributes of shape memory alloys, basically the materials capacity to do work. Principally, under specific materials where a huge part of the change strain is accommodated plastically. The mix of structure, thermodynamic and mechanical properties are utilized as devices to comprehend deformation and propose conceivable deformation mechanical while recognize possible target area for future alloy improvement [52].

1.3 Organization of Thesis

Chapter 1 includes the introduction and the properties of shape memory materials.

Chapter 2 includes the theoretical frameworks and literature review on the research topic.

Chapter 3 includes the simulations and analyses run to visualize the effect of forces on spring.

Chapter 4 includes the results and discussion.

Chapter 5 includes the conclusion and future work.

CHAPTER 2

THEORETICAL FRAMEWORK

2.1 Design of a Spring

Spring is an important machine element that comes in action whenever rigidity and small defections are required provided that it does not undermine the functionality of the product. Flexibility is usually required when internal machine parts needs to be controlled. These flexibility is attained by store and release of energy on application of force or torque on the spring [53].

Usually springs are classified as follow:

1. Wire springs
2. Flat springs
3. Special-shaped springs

The first type of spring include helical springs of round and square wires which can withstand under compressive, tensile or compressional loads. Wound motor- or clock-type power springs, Cantilever and elliptical springs, flat spring washers are the types of flat springs also known as Belleville springs [54].

2.2 Stresses in a Spring

The process of evaluation of stress in spring begins with defining parameter. Let *d* and *D* are the *wire diameter* and *mean coil diameter* respectively. A spring is shown in Figure 2.1**(a)** is loaded with axial force *F*. A section of spring in Figure 2.1**(b)** is taken from it and in the state of equilibrium, the shear force acting on it is F and torsional moment acting is $T = FD/2$.

The shear stress that could appear in this situation is evaluated by adding the shear force and the torsional force as follow:

$$\tau_{\max} = \frac{Tr}{J} + \frac{F}{A} \tag{2.1}$$

This shear stress appears at the inner side of the spring.

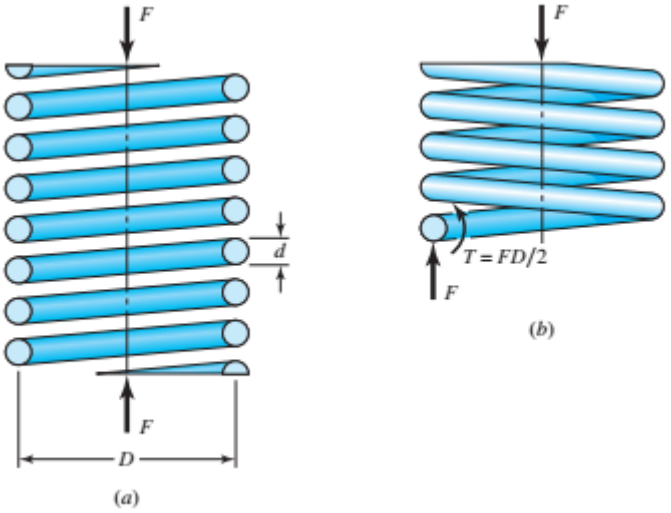

Figure 2.1 (*a*) Spring with axial load; **(*b*)** free-body diagram of spring under a direct shear and a torsional shear [54].

Doing the following suitable substitutions in Eq. (2.1):

$$\tau_{\max} = \tau \quad T = FD/2 \quad r = d/2 \quad J = \pi d^4/32 \quad A = \pi d^2/4 \tag{2.2}$$

The Eq. (2.1) becomes:

$$\tau = \frac{8FD}{\pi d^3} + \frac{4F}{\pi d^2} \tag{2.3}$$

Assuming the *spring index* as

$$C = \frac{D}{d} \tag{2.4}$$

It is the computation of coil curvature. Using Eq. (2.3) and Eq. (2.4) together yields:

$$\tau = K_s \frac{8FD}{\pi d^3} \tag{2.5}$$

where K_s is shear–correction factor and is as follow:

$$K_s = \frac{2C+1}{2C} = 1 + \frac{1}{2C} \tag{2.6}$$

2.3 Curvature Effect of a Spring

The Eq. (2.5) is used when the wire is straight which not the case is in helical spring hence, curvature of the wire is the reason of increase in stress on the inner side of the spring coil. It is applicable in the same way as stress correction factor. In case of static loading, this factor is meaningless since it causes strain hardening while in dynamic loading, which usually the normal function of spring is, the fatigue needs it to be included in the stress evaluation [55].

It is important to find curvature factor for the section of the spring but it is usually found through direct shear stress. Assuming K_s in Eq. (2.5) is replaced by K which can solve both issues of curvature and direct shear then it can be defined as

$$K_W = \frac{4C-1}{4C-4} + \frac{0.615}{C} \tag{2.7}$$

$$K_B = \frac{4C+2}{4C-3} \tag{2.8}$$

The factor represented by Eq. (2.7) is known as *Wahl factor* and the factor represented by Eq. (2.8) is known as *Bergsträsser factor*. Both factors differ by 1% hence Eq. (2.8) is better to use. The true curvature factor is obtained by cutting out the effect of direct shear stress [56]. By using Eq. (2.8) with Eq. (2.6), the curvature correction factor is given by

$$K_c = \frac{K_B}{K_s} = \frac{2C(4C+2)}{(4C-3)(2C+1)} \tag{2.9}$$

To include all stress-correction factors, simply multiply these with Eq. (2.5)

$$\tau = K_B \frac{8FD}{\pi d^3} \tag{2.10}$$

This is the maximum shear stress that appears on the spring.

2.4 Deflection in a Spring

The relation of deflection and force can be obtained by *Castigliano's theorem*. The total strain energy of a spring consists of summation of shear and torsional components. Hence the strain energy is

$$U = \frac{T^2 l}{2GJ} + \frac{F^2 l}{2AG} \tag{2.11}$$

Replacing the following substitutions:

$$T = FD/2 \quad l = \pi DN \quad J = \pi d^4/32 \quad A = \pi d^2/4 \tag{2.12}$$

The result of strain energy Eq. (2.11) becomes:

$$U = \frac{4F^2 D^3 N}{d^4 G} + \frac{2F^2 DN}{d^2 G} \tag{2.13}$$

In the above relation of strain energy, $N = N_a =$ number of active coils . Applying *Castigliano's theorem* to evaluate deflection *y*:

$$y = \frac{\partial U}{\partial F} = \frac{8FD^3 N}{d^4 G} + \frac{4FDN}{d^2 G} \tag{2.14}$$

Using Eq. (2.4) with Eq. (2.14)

$$y = \frac{8FD^3 N}{d^4 G}\left(1 + \frac{1}{2C^2}\right) \approx \frac{8FD^3 N}{d^4 G} \tag{2.15}$$

The parameter *spring rate* is also known as *scale* of the spring, which is $k = F/y$, and can be defined as

$$k \approx \frac{d^4 G}{8D^3 N} \tag{2.16}$$

2.5 Stability of a Spring

When the axial force is applied on a structure, it buckles. Same is the case with the spring, if the axial force is too large, the spring will buckle [57]. To avoid this, critical deflection y_{cr} is given as:

$$y_{cr} = L_0 C_1' \left(1 - \sqrt{1 - \frac{C_2'}{\lambda_{\text{eff}}^2}}\right) \tag{2.17}$$

Samónov [58] stated that Eq. (2.17) was used by Wahl [59] and the same equation is experimentally verified by Haringx [60, 61]. The factor λ_{eff} in Eq. (2.17) is known as *effective slenderness ratio* and is specified by:

$$\lambda_{\text{eff}} = \frac{\alpha L_0}{D} \tag{2.18}$$

Whereas the factors C_1' and C_2' are dimensionless elastic constants given by:

$$C_1' = \frac{E}{2(E-G)} \tag{2.19}$$

$$C_2' = \frac{2\pi^2(E-G)}{2G+E} \tag{2.20}$$

The Eq. (2.18) contains a factor α known as end-condition constant which depends upon the method of support on the ends of spring. The table represents the normal values for α

Table 2.1: End Condition of a Spring

End Condition	**Constant *α***
Support is flat parallel plate	0.5
One end supported by plane at right angle to spring axis	0.707
Both ends hinged	1
One end free; other end clamped	2

For the stability to be absolute, the term $C'_2/\lambda_{\text{eff}}^2$ in Eq. (2.17) must be greater than 1. This condition is met if and only if

$$L_0 < \frac{\pi D}{\alpha}\sqrt{\frac{2(E-G)}{2G+E}} \tag{2.21}$$

For conventional materials (steel), this condition is as follow:

$$L_0 < 2.63\frac{D}{\alpha} \tag{2.22}$$

For ground and squared ends which is supported by flat parallel planes, $\alpha = 0.5$ and $L_0 < 5.26D$.

2.6 Spring Materials

Springs are usually manufactured by the following processes:

1. Hot working
2. Cold working

The process of making spring depends upon the spring index and the size of the material. If the spring index $C = D/d < 4$ or if $d > 1/4$ in , then wire is not generally pre-hardened. When sping wire in wound, it causes residual stresses due to bending but these are at right angle to the torsional working stress. This residual stress is often relieved by minor heat treatment [62].

There are various materials suited for spring manufacturing including alloy steels, carbon steels and corrosion-resisting steels besides nonferrous materials like bronze, beryllium, phosphorous, copper, spring brass and many nickel based alloys [63].

The material of springs are compared by tensile strength but this differs with length of spring wire and hence true strength cannot be known unless the diameter of wire *d* is known. To capture this problem, a plot of tensile strength against wire diameter is drawn which is approximately a straight line when drawn on log-log graph [64]. The equation of the relation between two variables is

$$S_{ut} = \frac{A}{d^m} \tag{2.23}$$

Eq. (2.23) has *A* as an intercept and *m* as slope. It gives the least tensile strength of the spring material under consideration. Another factor, torsional yield strength is also required to estimate the strength of the spring material but generally spring material is passed on tensile strength only. It is because, by a grave estimate, the tensile yield point is in between 60 – 90 %

of tensile strength [65]. According to *Distortion-Energy* theory, the torsional yield strength is approximated as $S_{sy} = S_y / \sqrt{3}$. This method gives the following result for steels:

$$0.35 \leq S_{sy} \leq 0.52 S_{ut} \tag{2.24}$$

CHAPTER 3

SIMULATIONS AND ANALYSES

3.1 3D Modelling

The spring is designed in a commercial 3D CAD package with following parameters (Table 3.1) and CAD model is shown in Figure 3.1.

Table 3.1 Parameters of spring

Parameter	**Value**
Wire diameter, *d* [mm]	2.16
Coil diameter, *D* [mm]	23.1
Number of Active coils, *n*	3
Initial free length, l_o [mm]	19

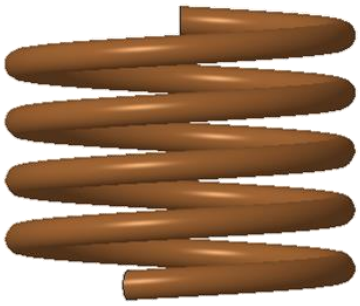

Figure 3.1 3D CAD model

The spring is loaded with axial loading *P* as shown in Figure 3.3 keeping the top of the spring fixed (Figure 3.4). The rest of the spring is constrained in *x*- and *z*-directions while free in *y*-direction (Figure 3.5).

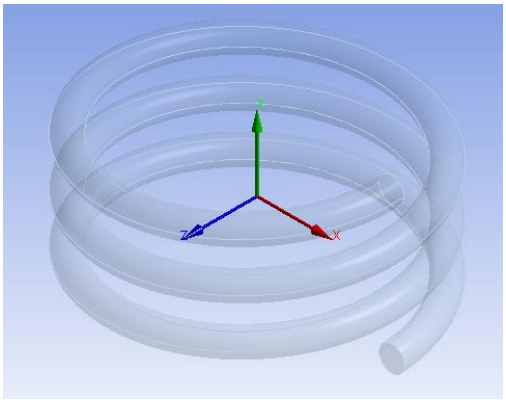

Figure 3.2 The coordinate system for simulation

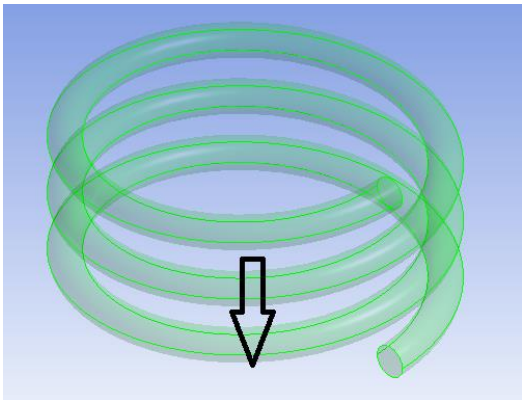

Figure 3.3 Force *P* applied on lower end of spring

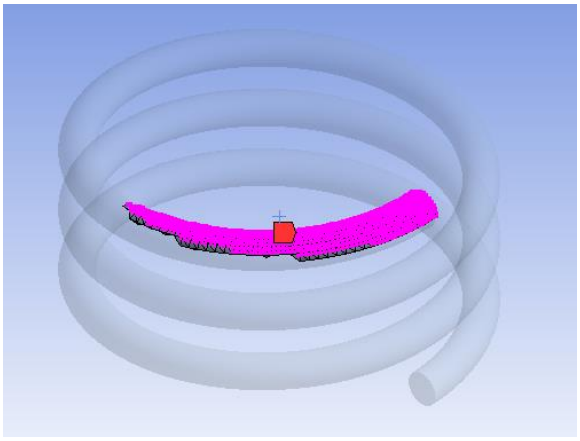

Figure 3.4 Fixed nodes in all directions

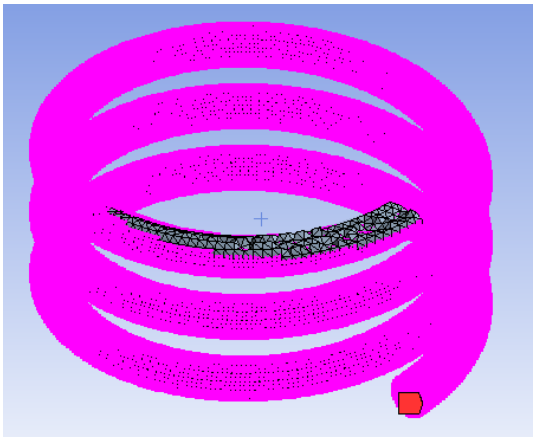

Figure 3.5 Fixed nodes in *x*- and *z*-directions and free in *y*- direction

Keeping axial load applied, the temperature is increased beyond transformation temperature to introduce thermal strain. Removing temperature loading followed by removal of axial loading.

The behaviour of NiTiPdPt and NiTiPdCu has been realized by conducting experiments. These results are compared with FEA results and extrapolated. The following plots displays the relation of stress, strain, displacement, temperature and energy dissipation per unit volume.

3.2 Simulations

3.2.1 SMAs under 40 N force

The following plots represent the results of $Ni_{19.5}Ti_{50.5}Pd_{25}Pt_5$ at 320 °C and $Ni_{15}Ti_{50}Pd_{25}Cu_{10}$ at 250 °C under force of ± 40 N.

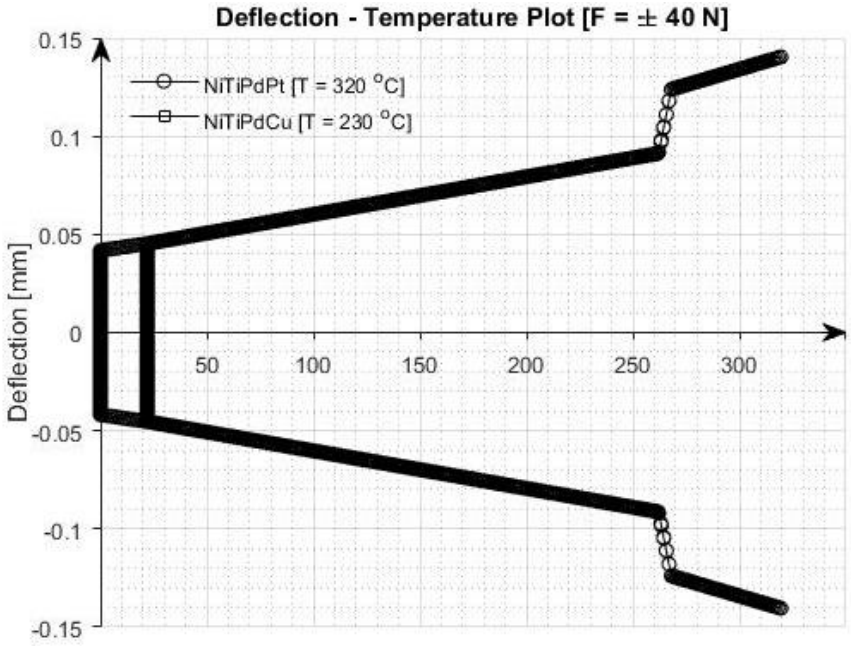

Figure 3.6 Deflection *vs*. Temperature for both SMAs under F = ± 40 N.

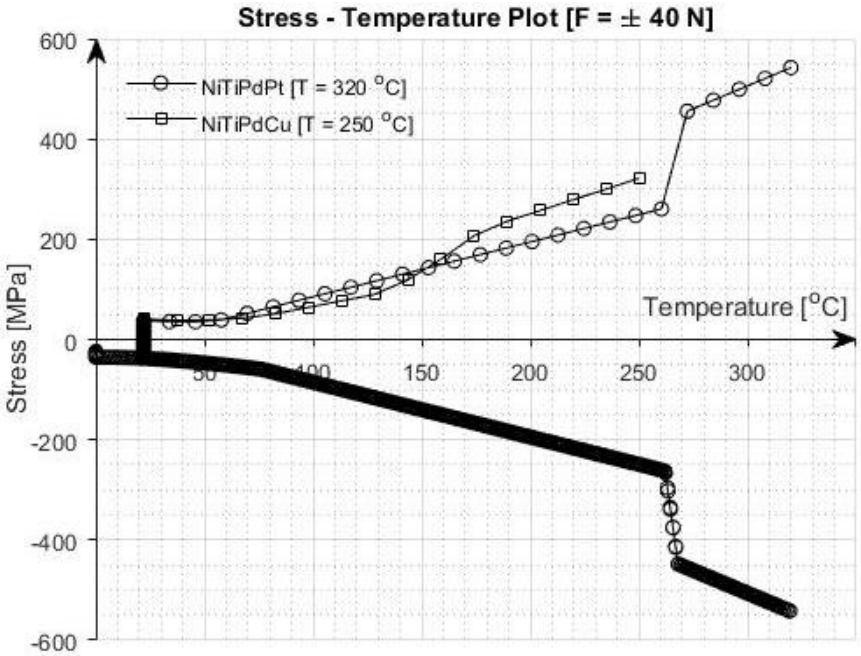

Figure 3.7 Stress *vs*. Temperature for both SMAs under F = ± 40 N.

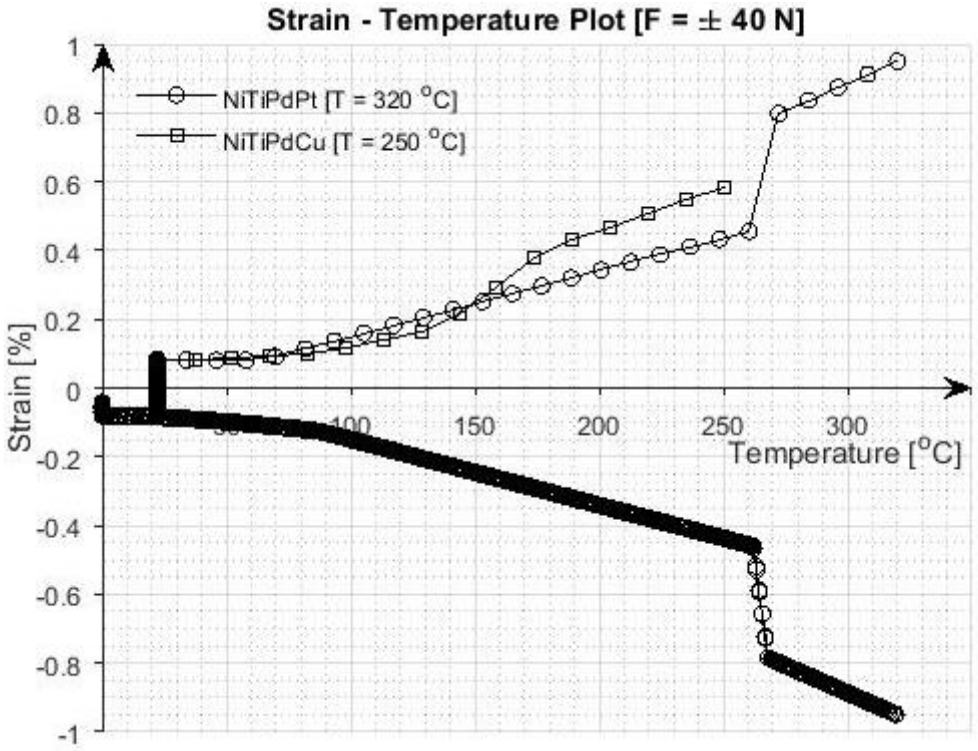

Figure 3.8 Strain *vs*. Temperature for both SMAs under F = ± 40 N.

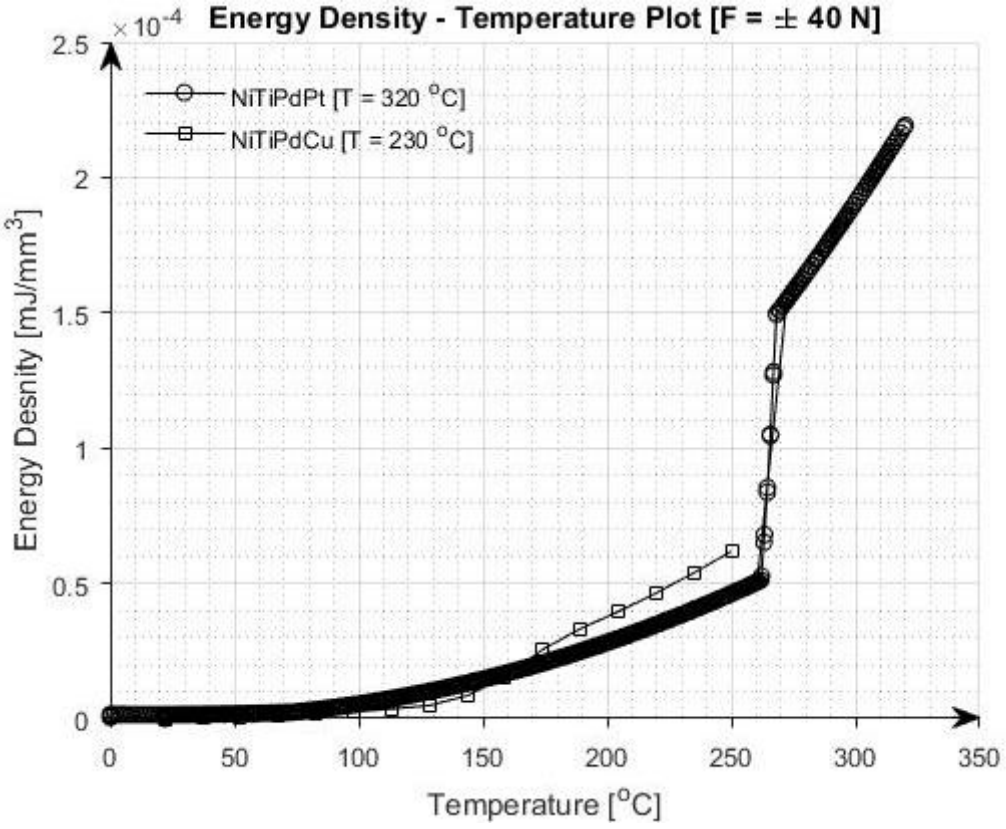

Figure 3.9 Energy density *vs*. Temperature for both SMAs under F = ± 40 N.

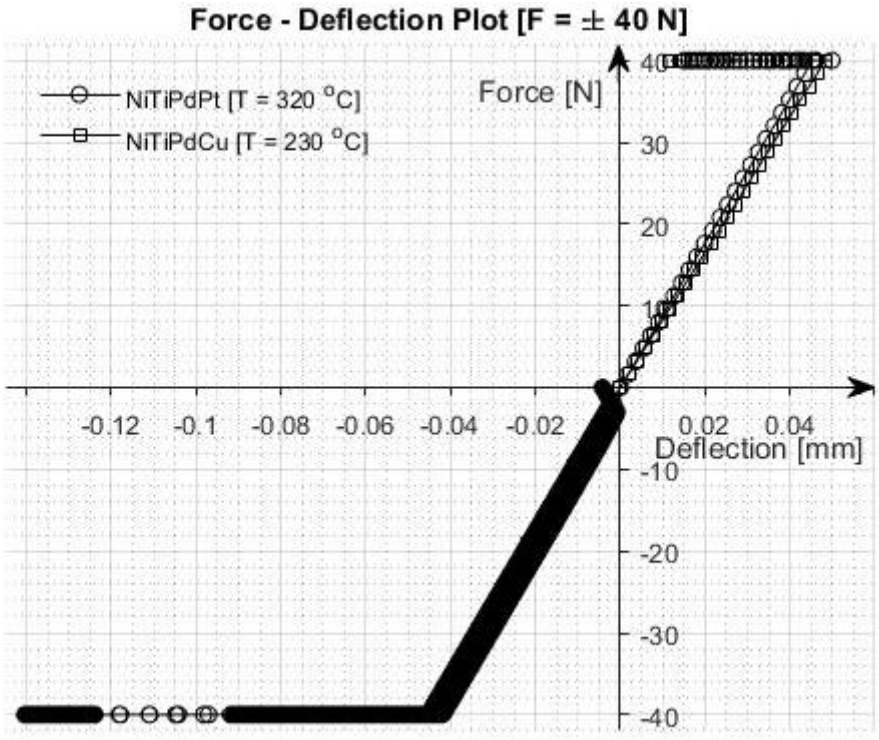

Figure 3.10 Force *vs*. Deflection for both SMAs under F = ± 40 N.

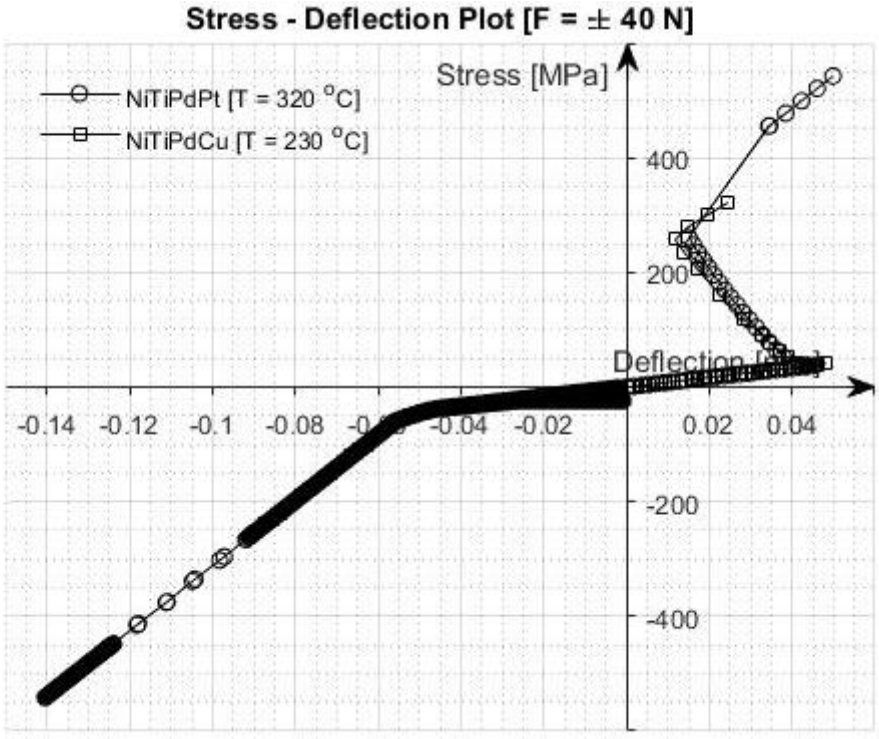

Figure 3.11 Stress *vs*. Deflection for both SMAs under F = ± 40 N.

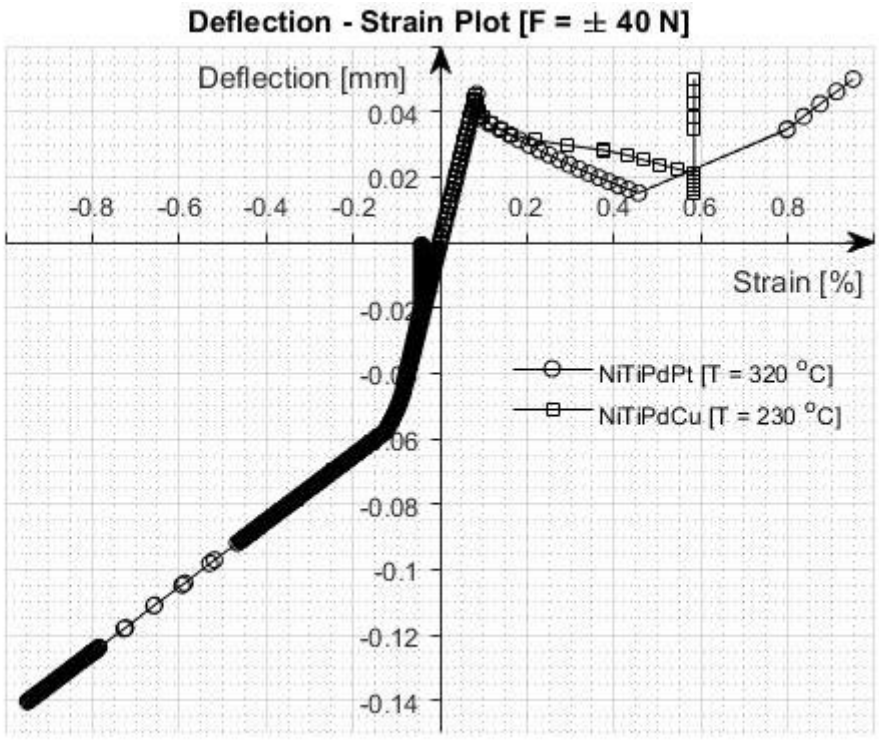

Figure 3.12 Deflection *vs*. Strain for both SMAs under F = ± 40 N.

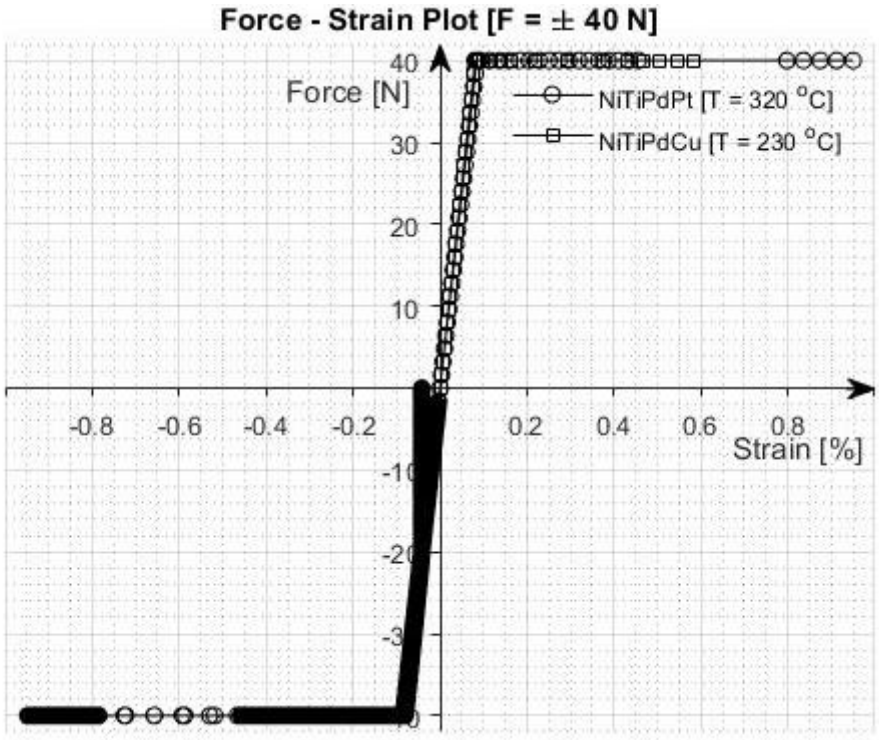

Figure 3.13 Force *vs*. Strain for both SMAs under F = ± 40 N.

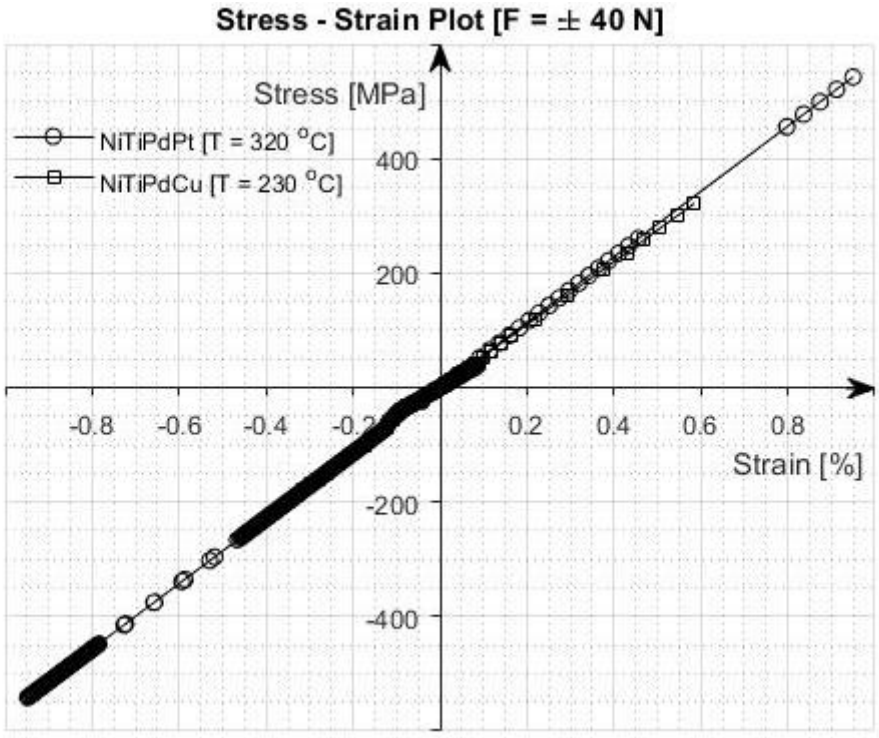

Figure 3.14 Stress *vs*. Strain for both SMAs under F = ± 40 N.

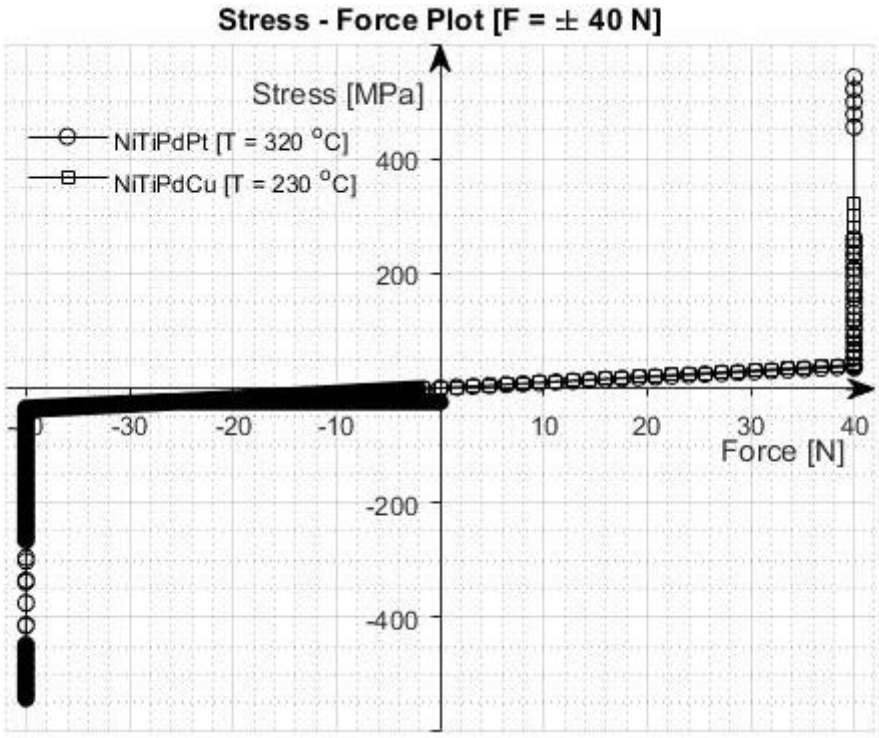

Figure 3.15 Stress *vs*. Force for both SMAs under F = ± 40 N.

3.2.2 SMAs under 100 N force

The following plots represent the results of $Ni_{19.5}Ti_{50.5}Pd_{25}Pt_5$ at 320 °C and $Ni_{15}Ti_{50}Pd_{25}Cu_{10}$ at 250 °C under force of ± 100 N.

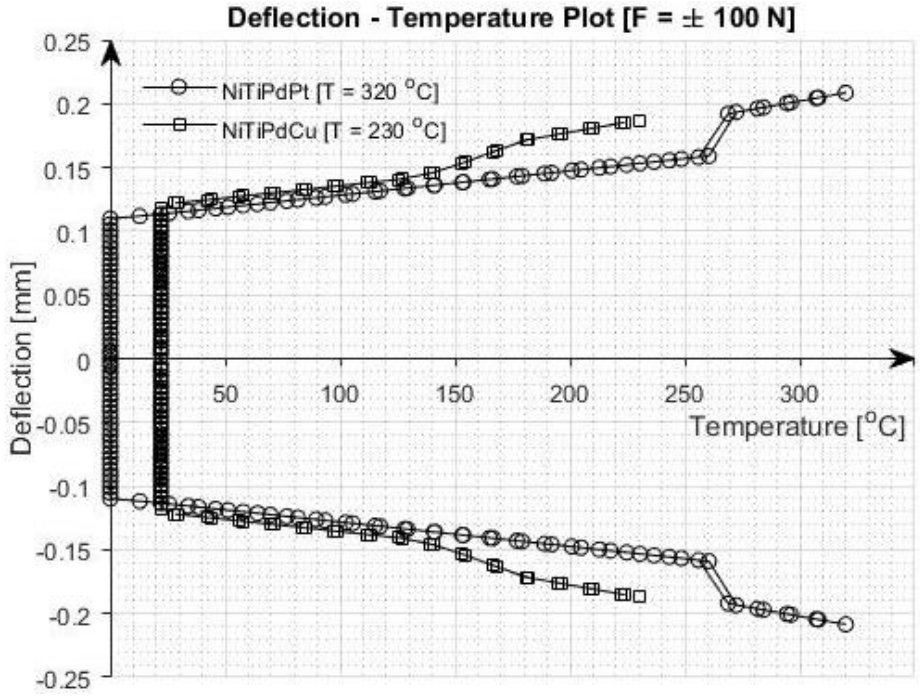

Figure 3.16 Deflection *vs*. Temperature for both SMAs under F = ± 100 N.

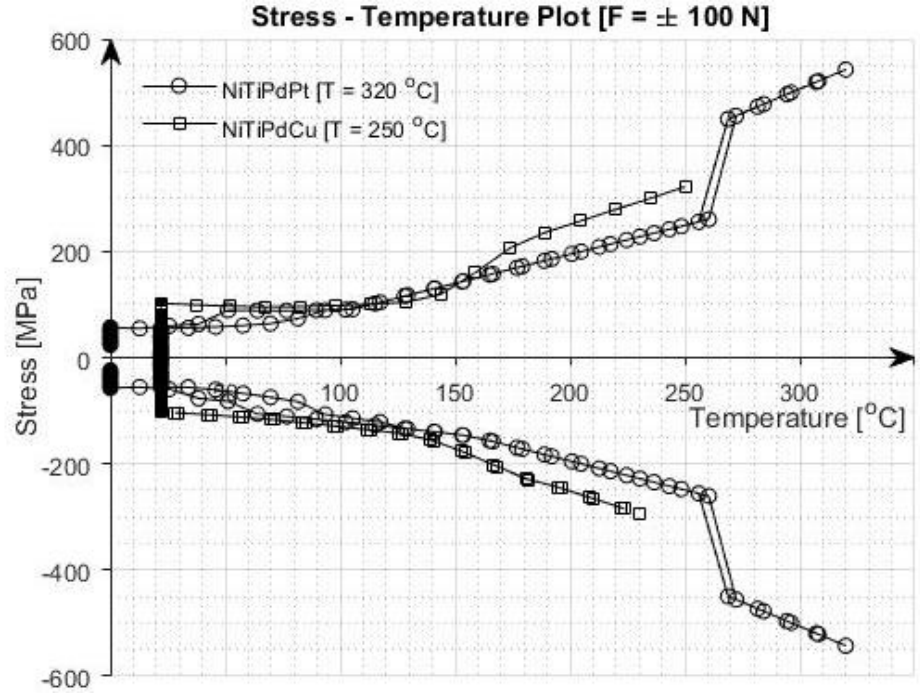

Figure 3.17 Stress *vs*. Temperature for both SMAs under F = ± 100 N.

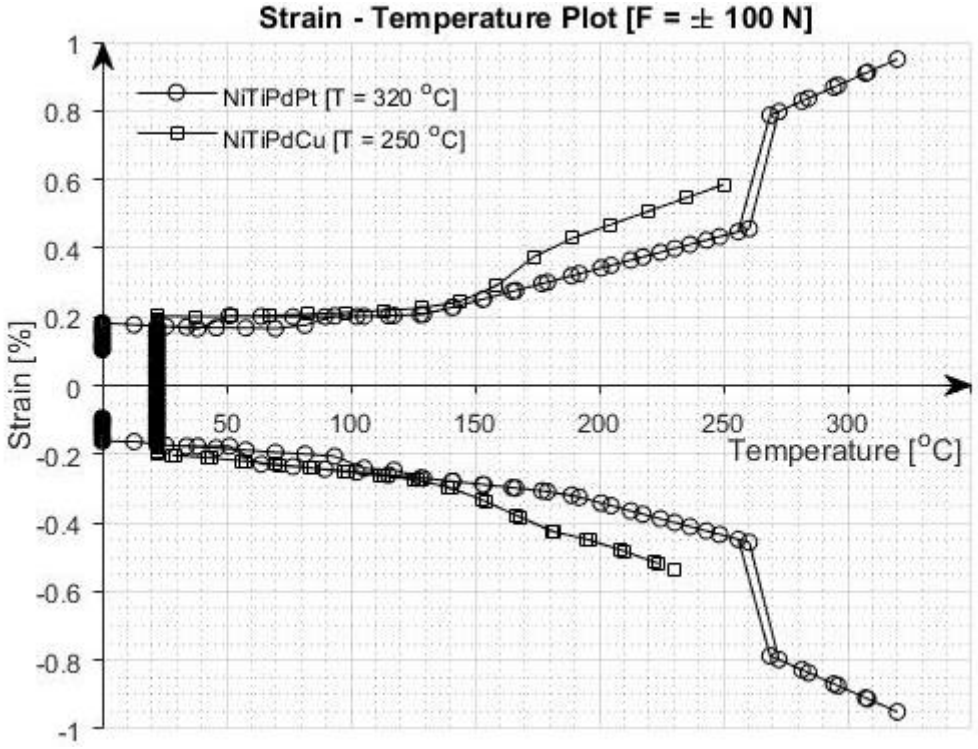

Figure 3.18 Strain *vs*. Temperature for both SMAs under F = ± 100 N.

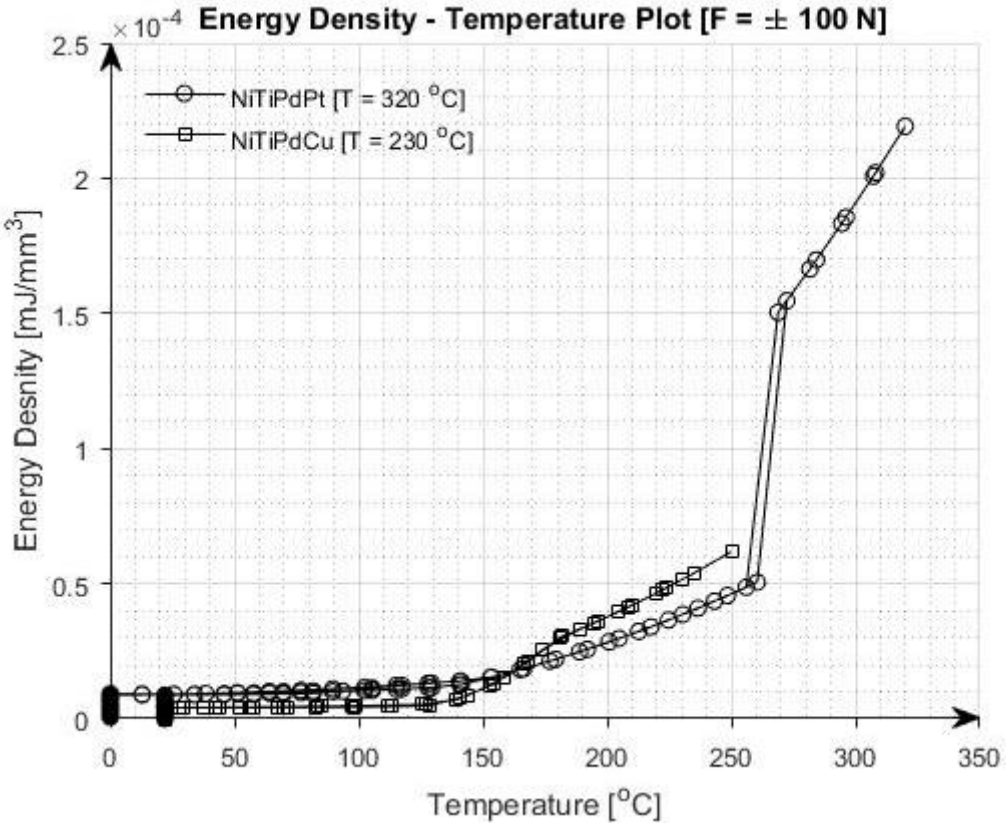

Figure 3.19 Energy density *vs*. Temperature for both SMAs under F = ± 100 N.

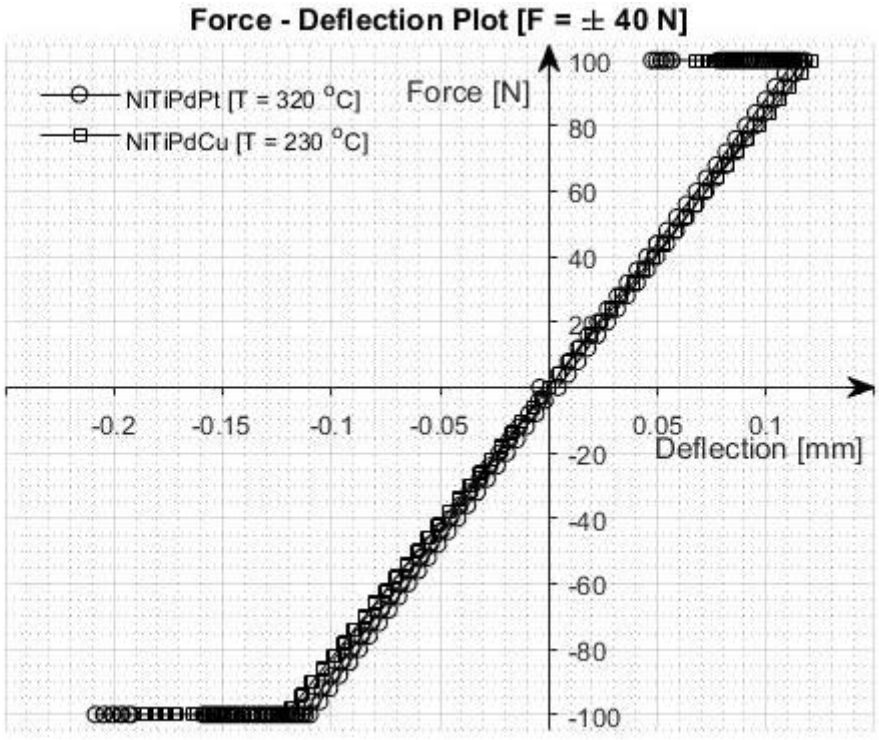

Figure 3.20 Force *vs*. Deflection for both SMAs under F = ± 100 N.

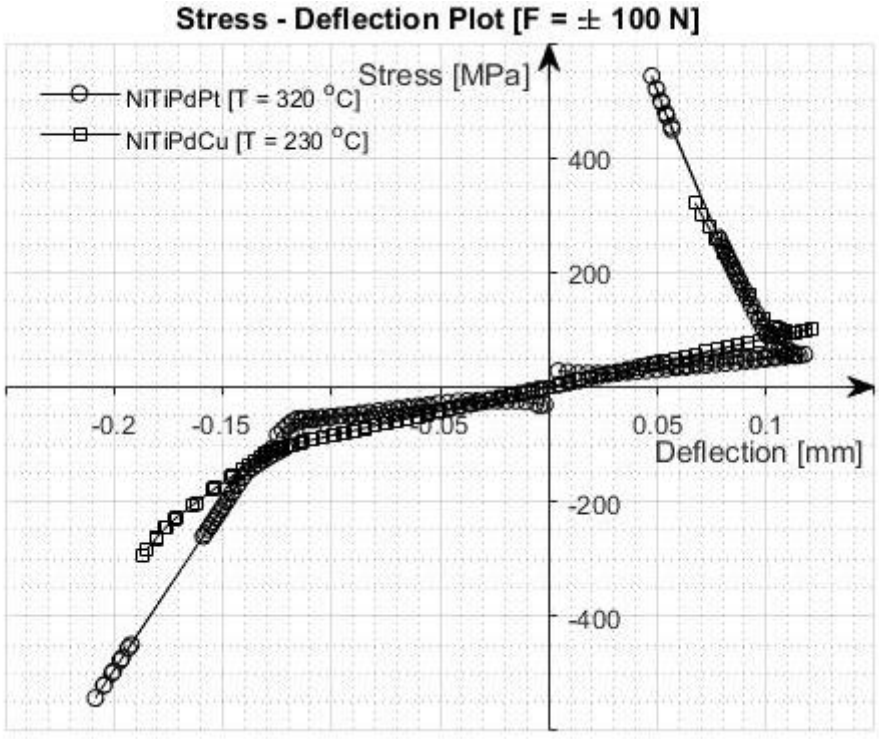

Figure 3.21 Stress *vs*. Deflection for both SMAs under F = ± 100 N.

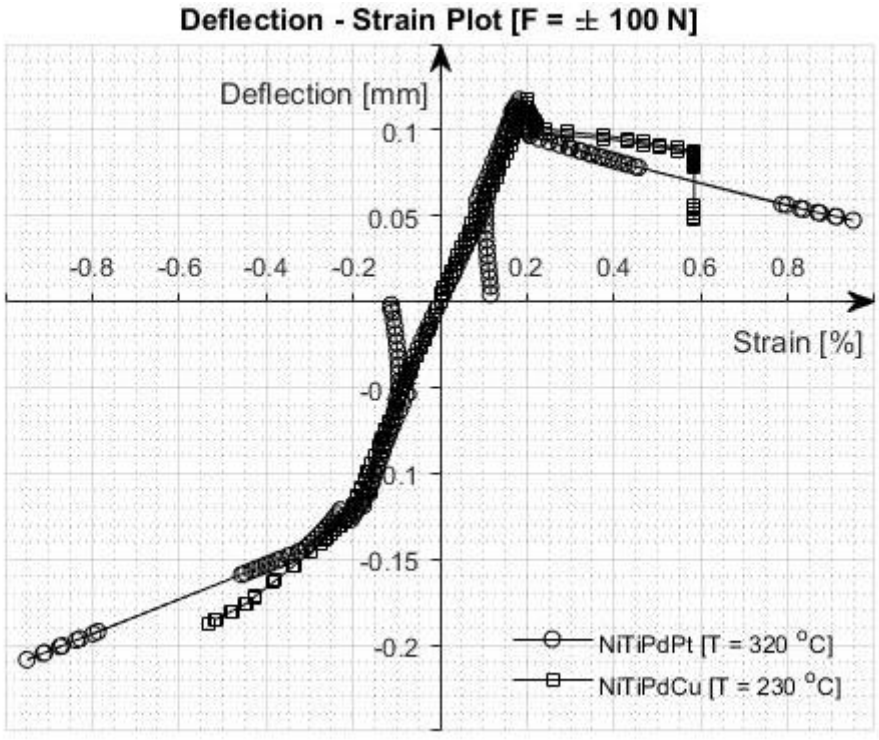

Figure 3.22 Deflection *vs*. Strain for both SMAs under F = ± 100 N.

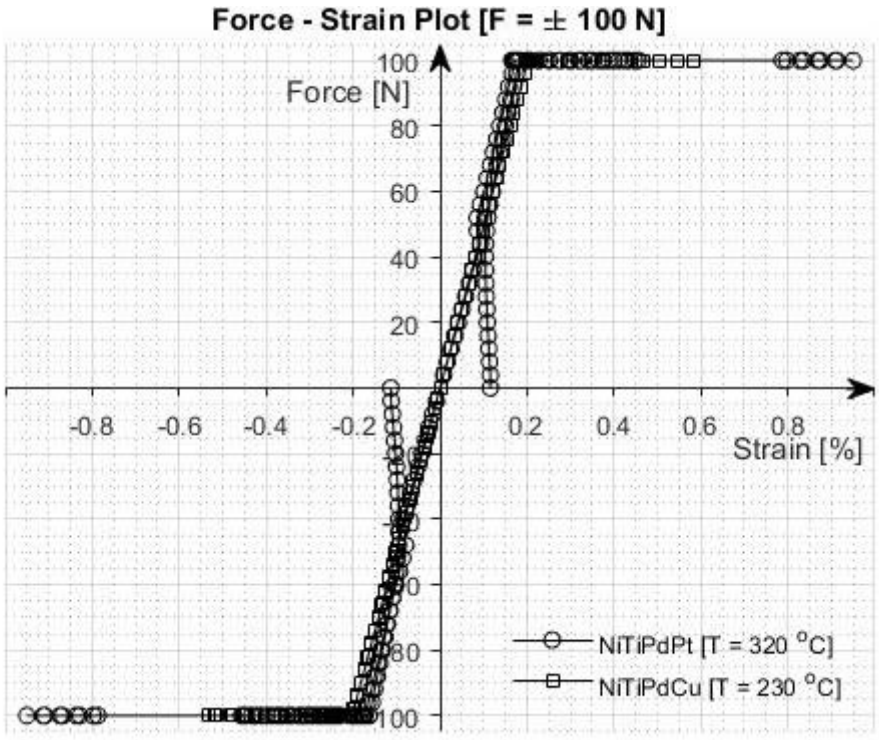

Figure 3.23 Force *vs*. Strain for both SMAs under F = ± 100 N.

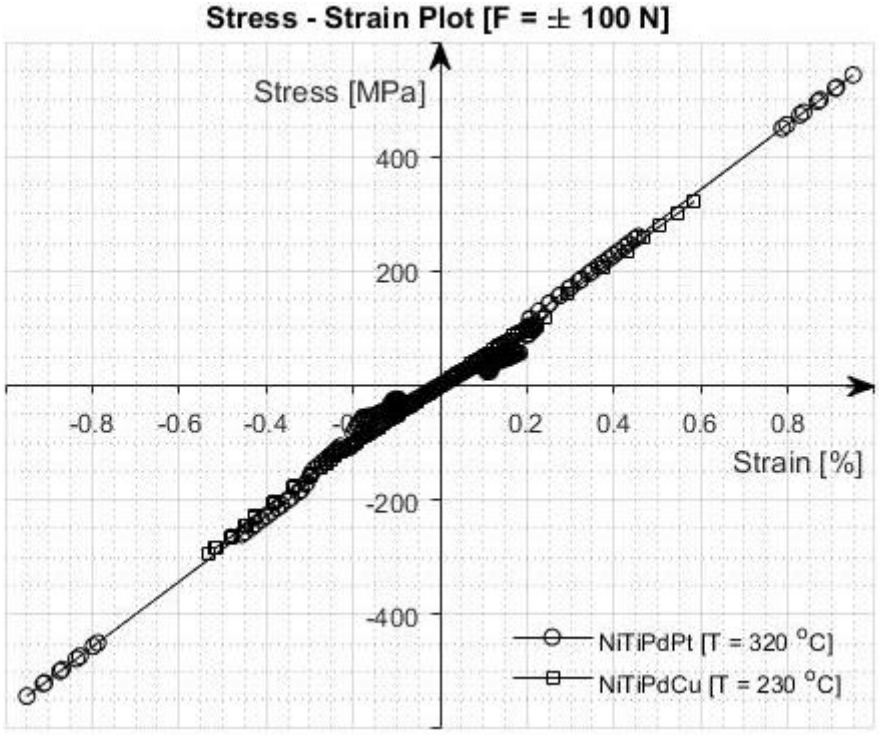

Figure 3.24 Stress *vs*. Strain for both SMAs under F = ± 100 N.

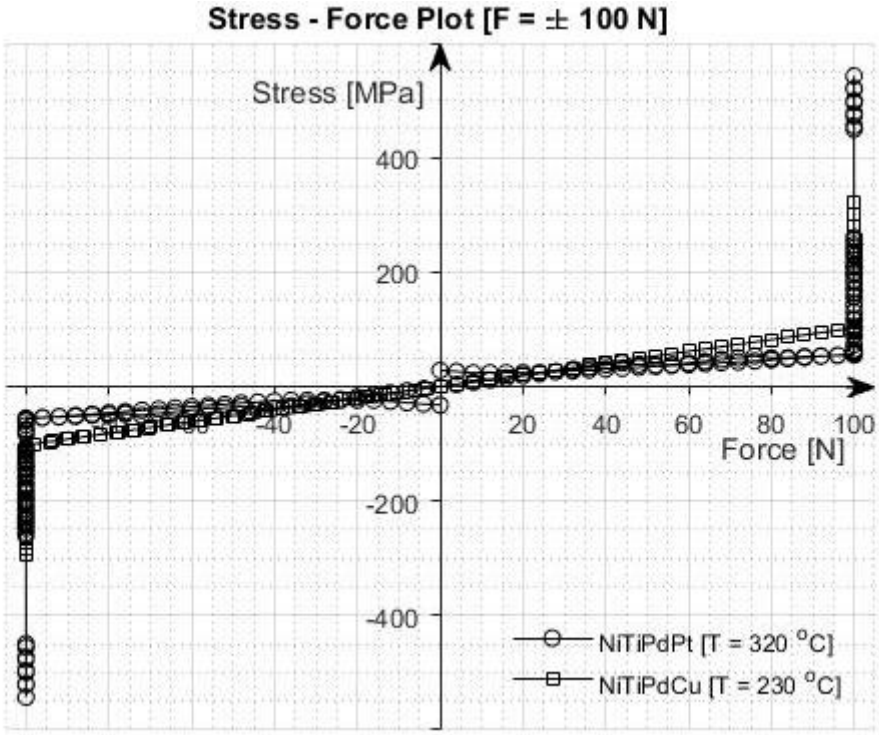

Figure 3.25 Stress *vs*. Force for both SMAs under F = ± 100 N.

3.2.3 NiTiPdPt under 125 N force

The following plots represent the results of $Ni_{19.5}Ti_{50.5}Pd_{25}Pt_5$ at 320 °C under force of ± 125 N.

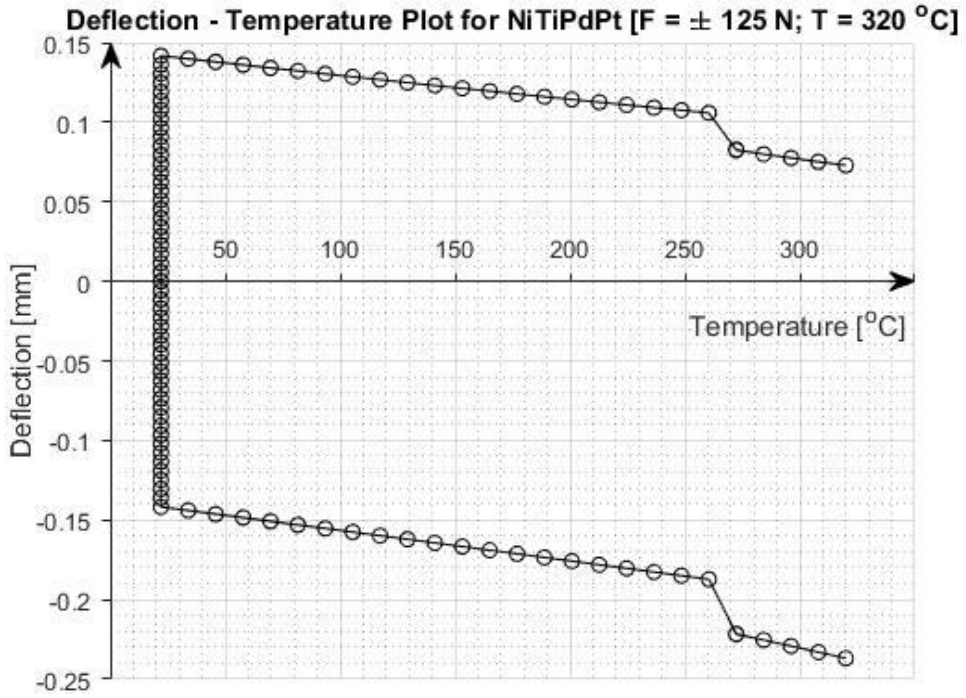

Figure 3.26 Deflection *vs*. Temperature for NiTiPdPt at 320 °C under F = ± 125 N.

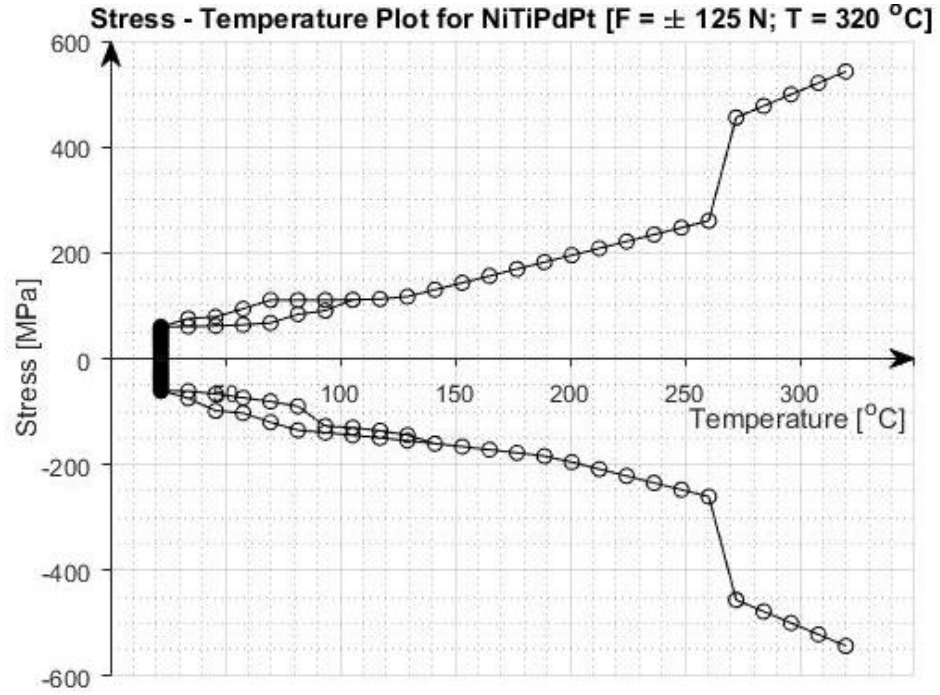

Figure 3.27 Stress *vs*. Temperature for NiTiPdPt at 320 °C under F = ± 125 N.

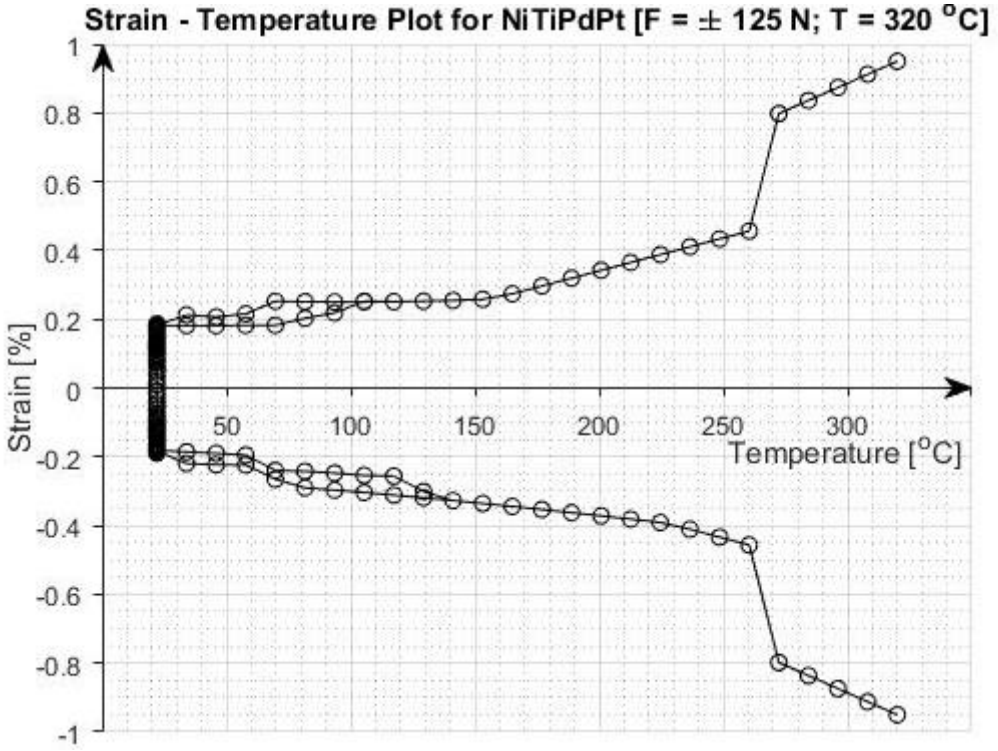

Figure 3.28 Strain *vs*. Temperature for NiTiPdPt at 320 °C under F = ± 125 N.

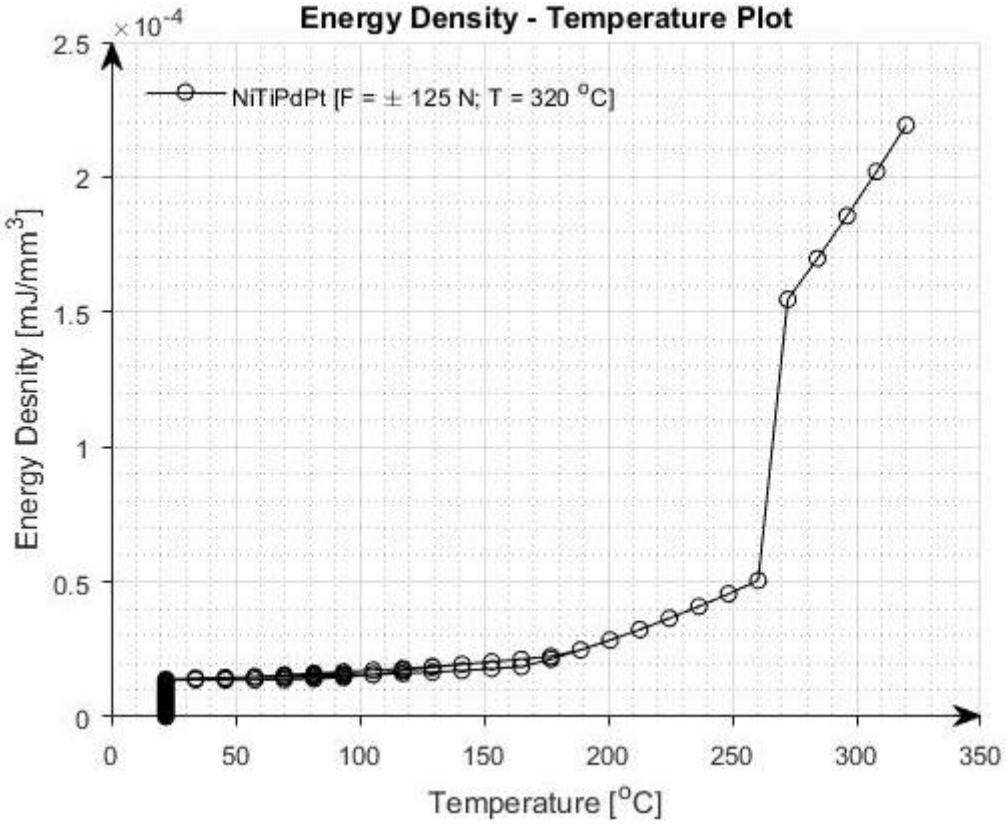

Figure 3.29 Energy density *vs*. Temperature for NiTiPdPt at 320 °C under F = ± 125 N.

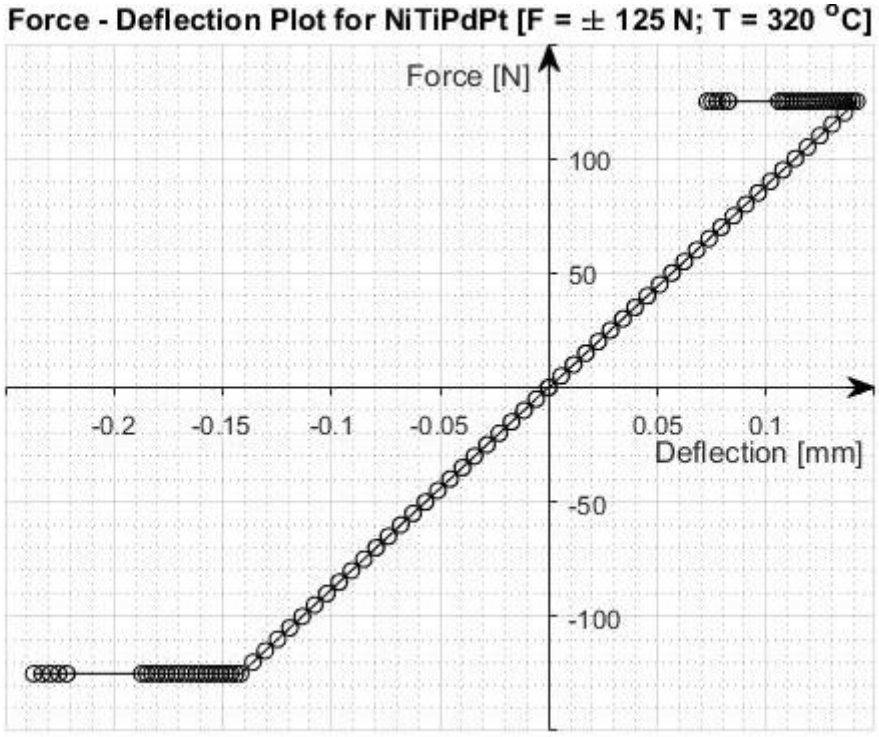

Figure 3.30 Force *vs*. Deflection for NiTiPdPt at 320 °C under F = ± 125 N.

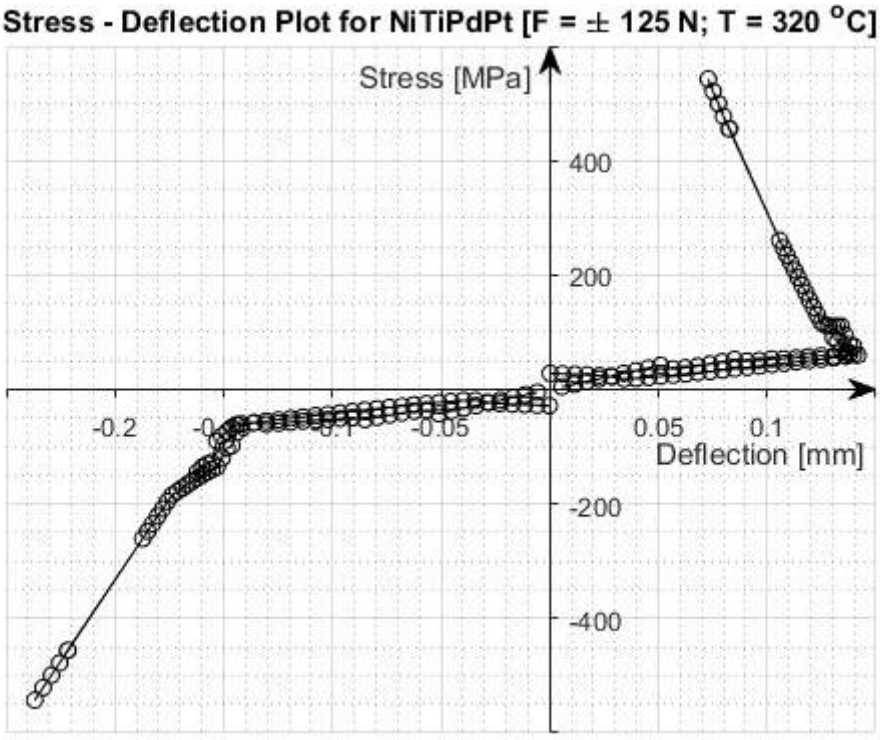

Figure 3.31 Stress *vs*. Deflection for NiTiPdPt at 320 °C under F = ± 125 N.

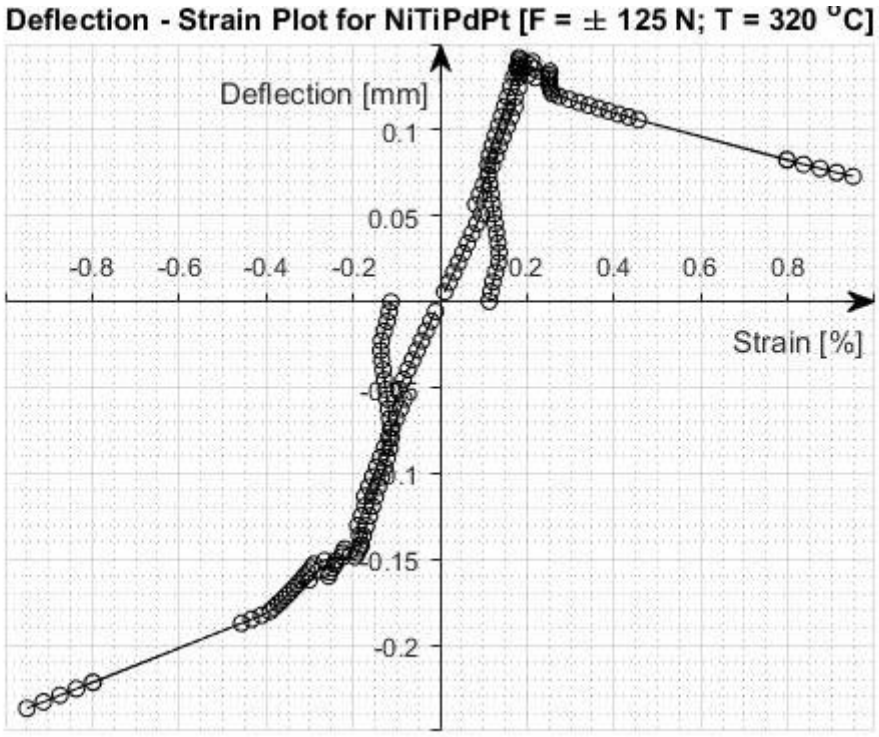

Figure 3.32 Deflection *vs*. Strain for NiTiPdPt at 320 °C under F = ± 125 N.

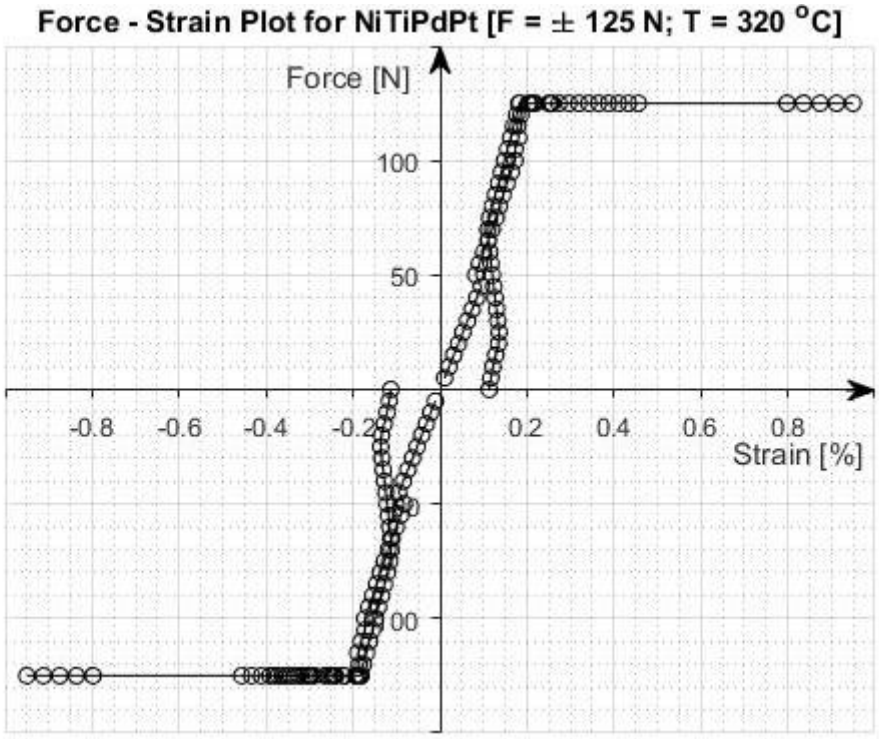

Figure 3.33 Force *vs*. Strain for NiTiPdPt at 320 °C under F = ± 125 N.

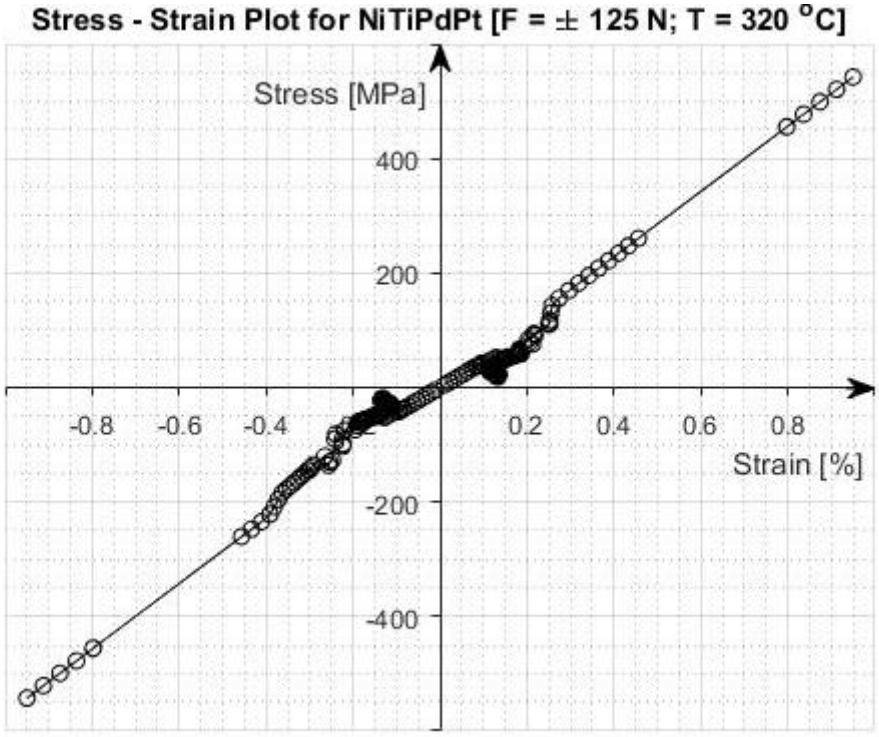

Figure 3.34 Stress *vs*. Strain for NiTiPdPt at 320 °C under F = ± 125 N.

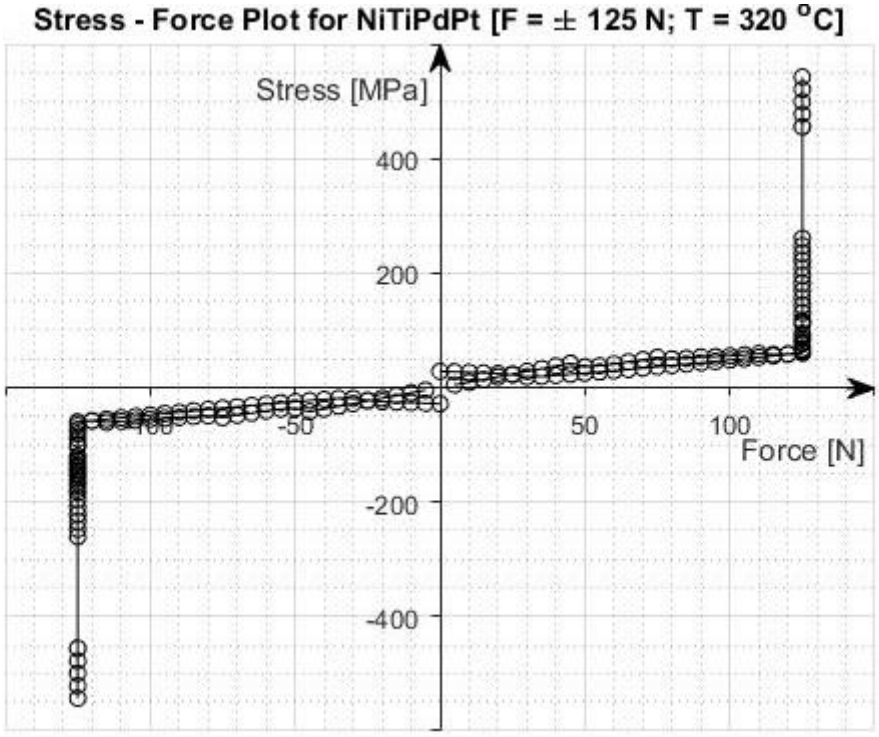

Figure 3.35 Stress *vs*. Force for NiTiPdPt at 320 °C under F = ± 125 N.

3.2.4 NiTiPdCu under 2000 N force

The following plots represent the results of $Ni_{15}Ti_{50}Pd_{25}Cu_{10}$ at 250 °C under force of 2000N

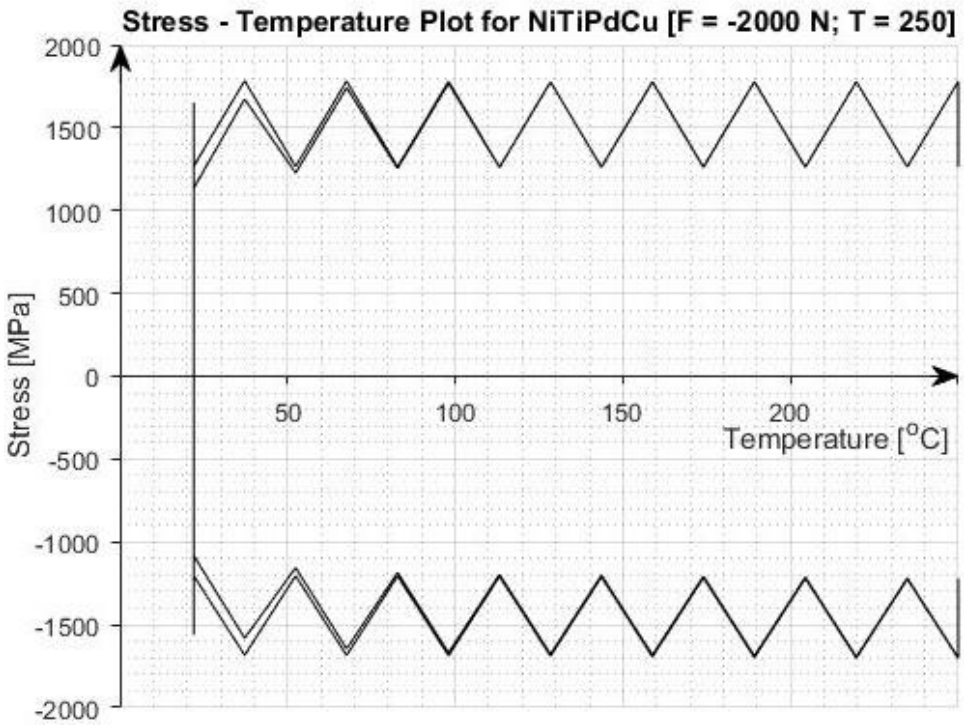

Figure 3.36 Stress *vs*. Temperature for NiTiPdCu at T = 250 °C under F = ± 2000 N.

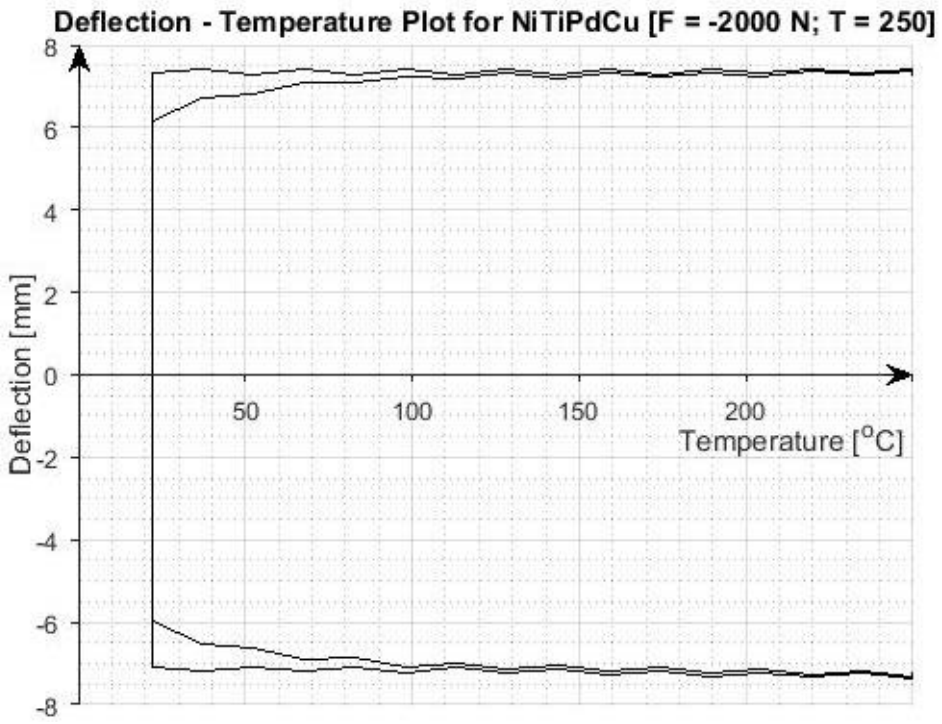

Figure 3.37 Defection *vs.* Temperature for NiTiPdCu at T = 250 °C under F = ± 2000 N.

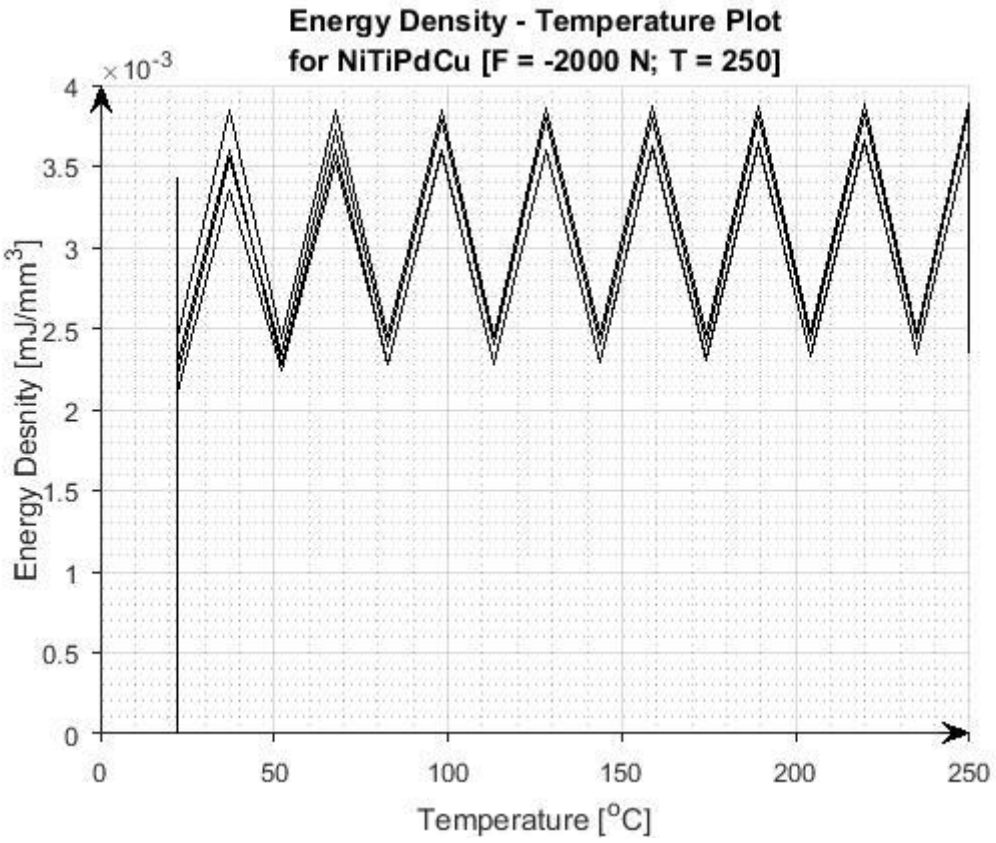

Figure 3.38 Energy density *vs.* Temperature for NiTiPdCu at T = 250 °C under F = ± 2000 N.

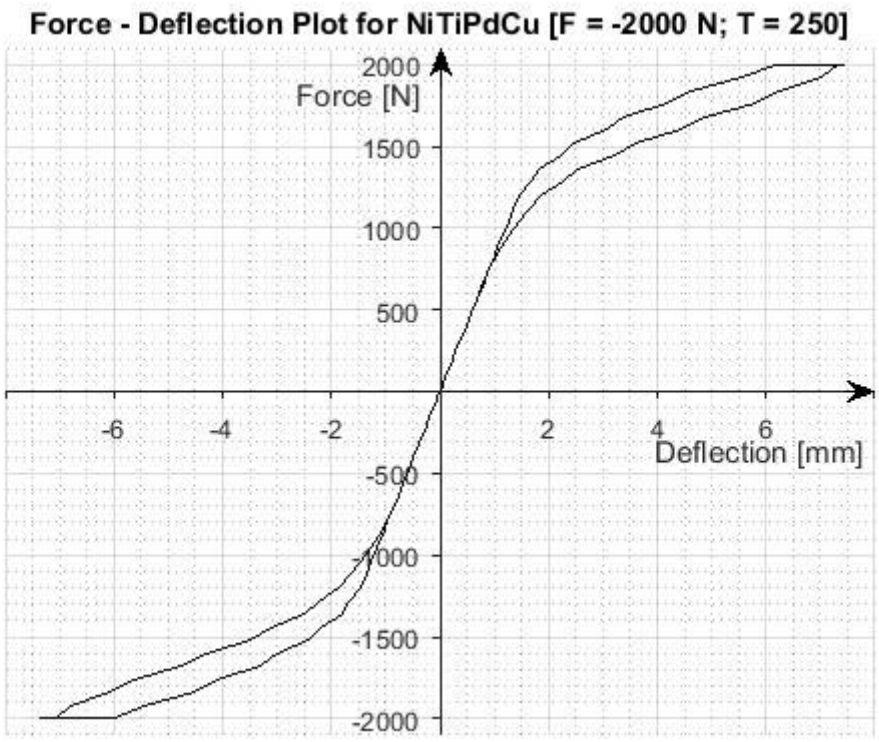

Figure 3.39 Force *vs.* Deflection for NiTiPdCu at T = 250 °C under F = ± 2000 N.

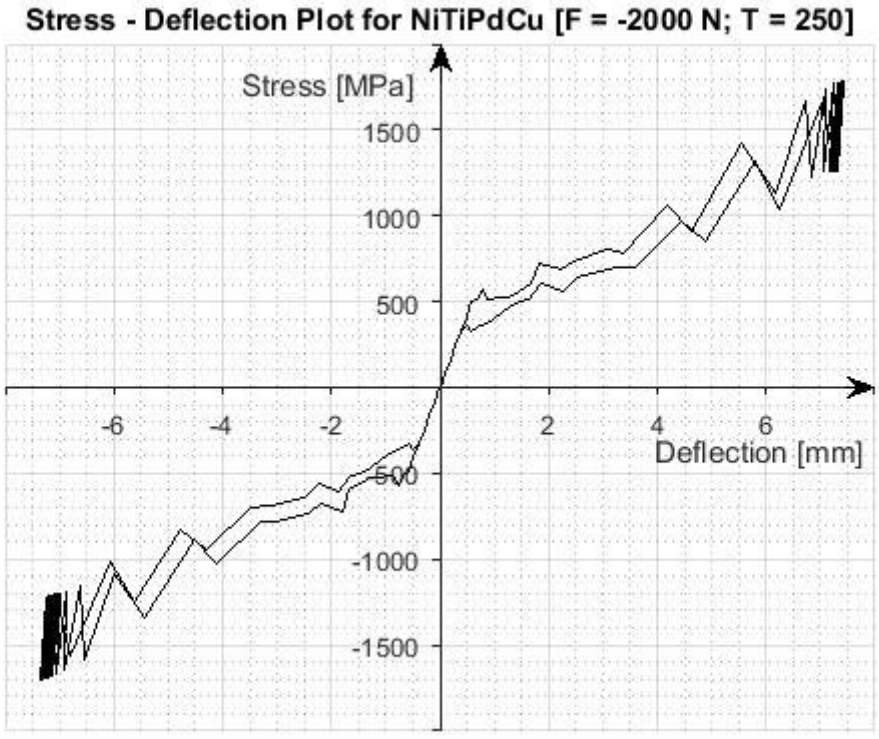

Figure 3.40 Stress *vs.* Defection for NiTiPdCu at T = 250 °C under F = ± 2000 N.

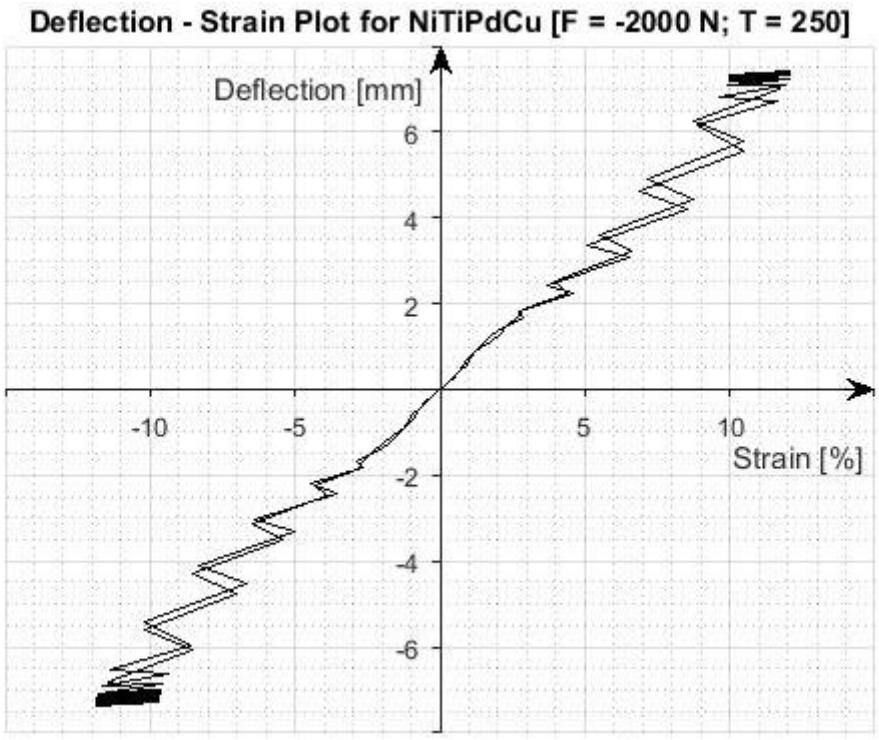

Figure 3.41 Deflection *vs.* Strain for NiTiPdCu at T = 250 °C under F = ± 2000 N.

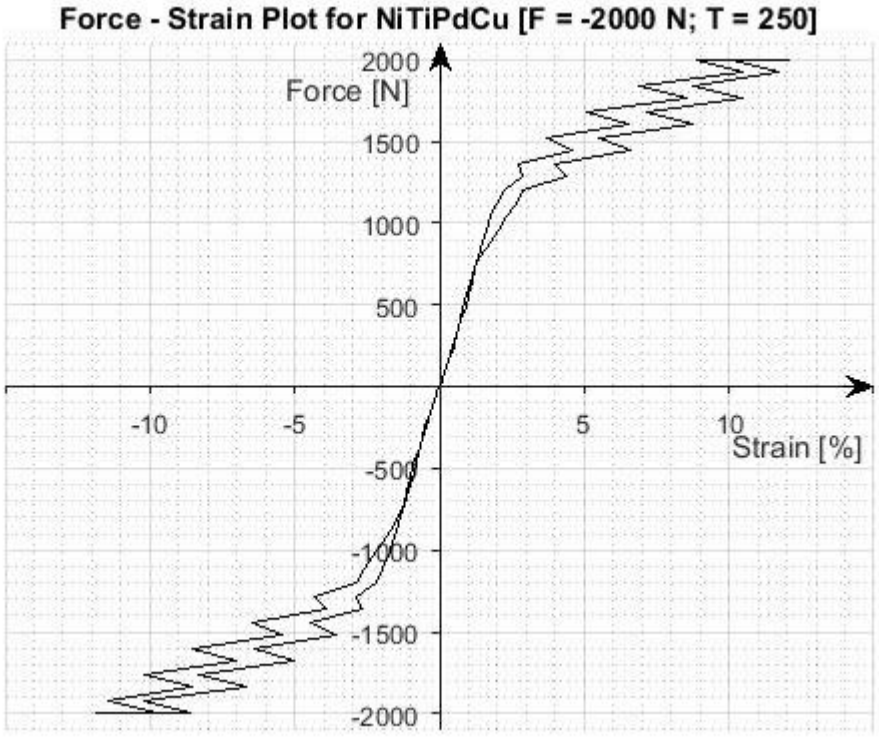

Figure 3.42 Force *vs.* Strain for NiTiPdCu at T = 250 °C under F = ± 2000 N.

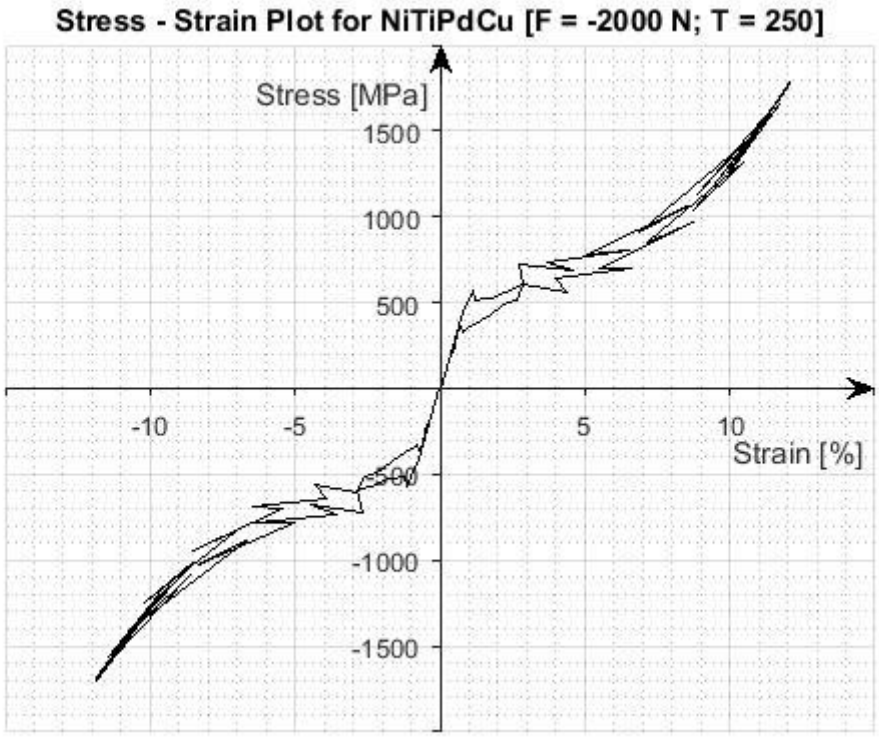

Figure 3.43 Stress *vs.* Strain for NiTiPdCu at T = 250 °C under F = ± 2000 N.

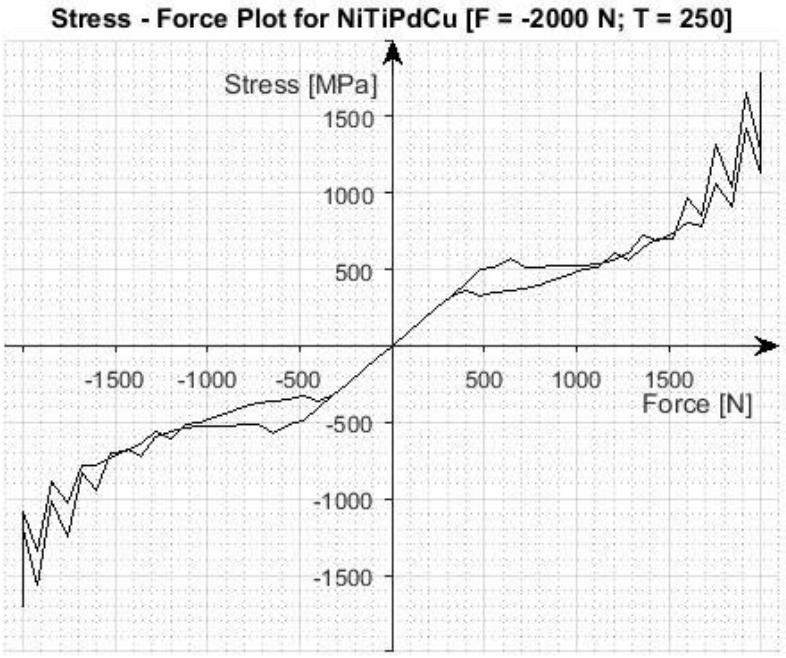

Figure 3.44 Stress *vs.* Force for NiTiPdCu at T = 250 °C under F = ± 2000 N.

3.2.5 NiTiPdCu under 0.50 and 0.75 Pa pressure

The following plots represent the results of $Ni_{15}Ti_{50}Pd_{25}Cu_{10}$ at 230 °C under pressure of 0.50 Pa and 0.75 Pa.

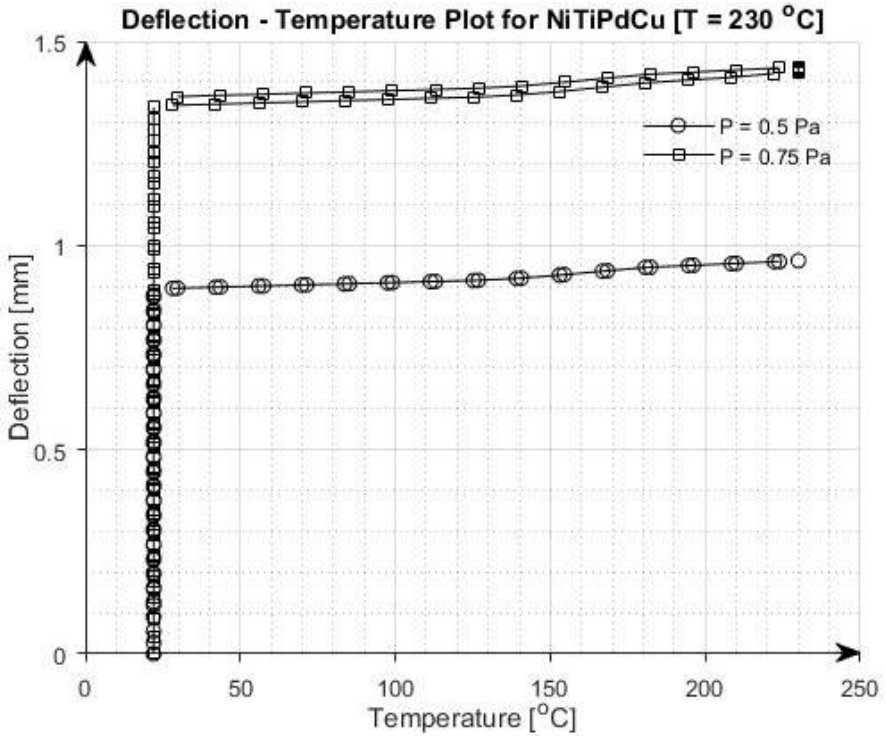

Figure 3.45 Deflection *vs.* Temperature for NiTiPdCu at T = 230 °C.

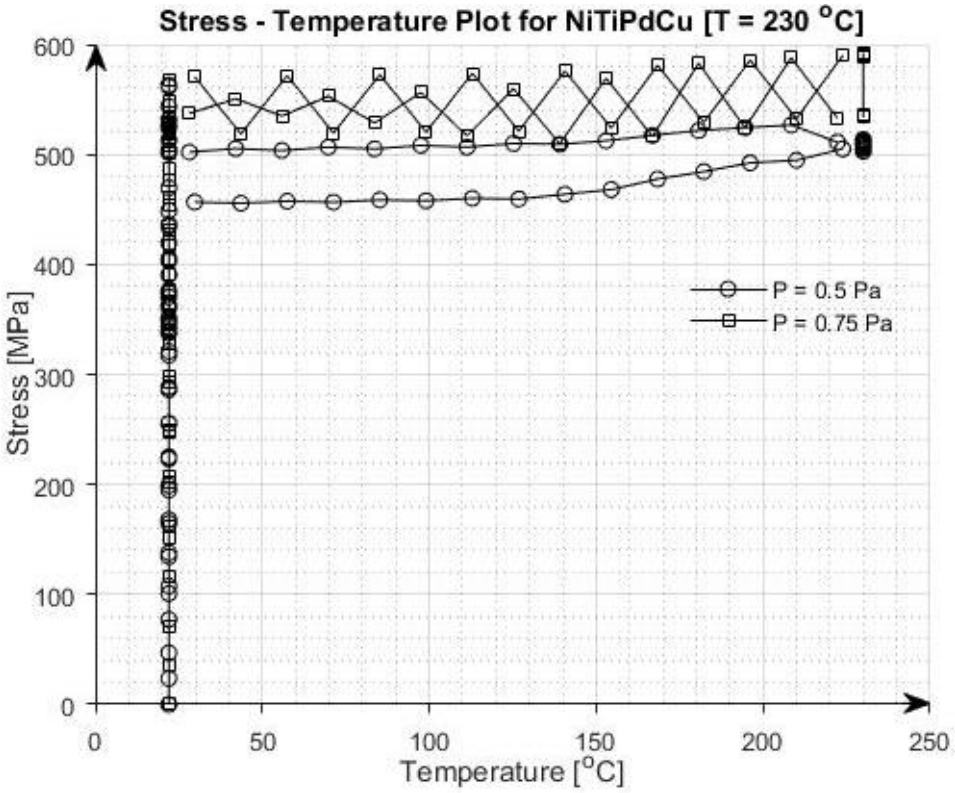

Figure 3.46 Stress *vs.* Temperature for NiTiPdCu at T = 230 °C.

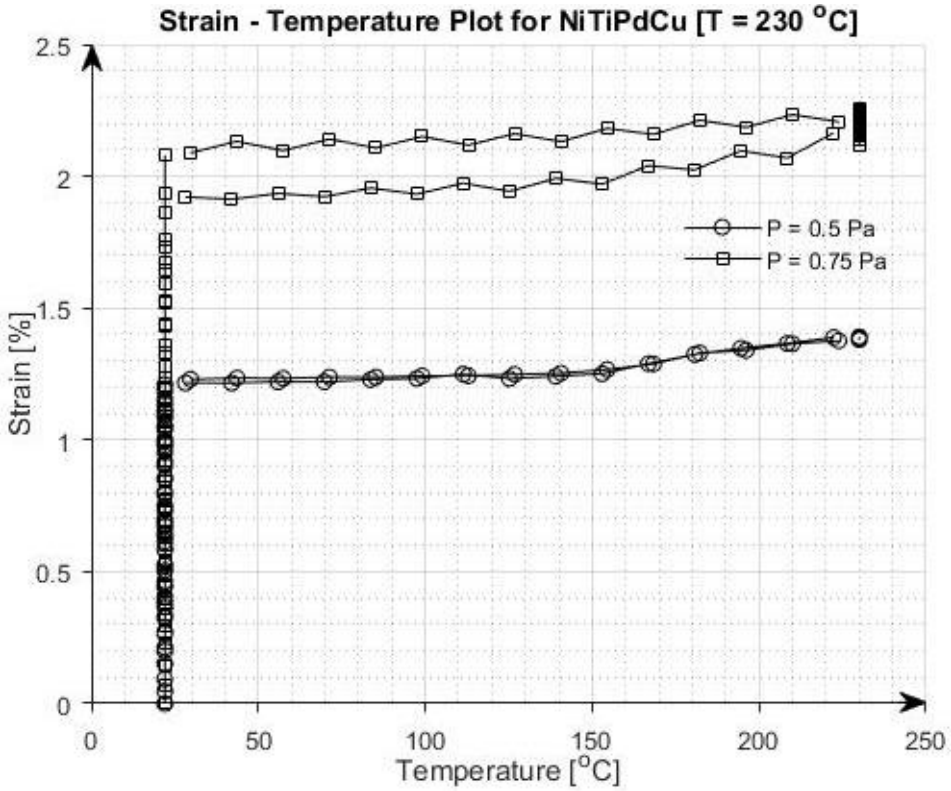

Figure 3.47 Strain *vs.* Temperature for NiTiPdCu at T = 230 °C.

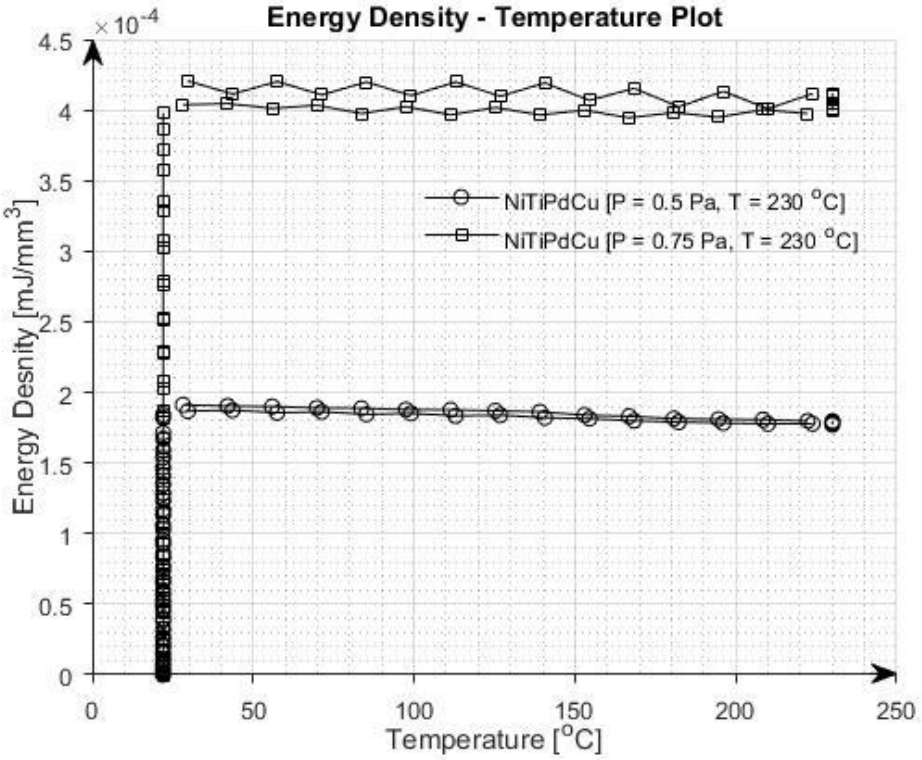

Figure 3.48 Energy density *vs.* Temperature for NiTiPdCu at T = 230 °C.

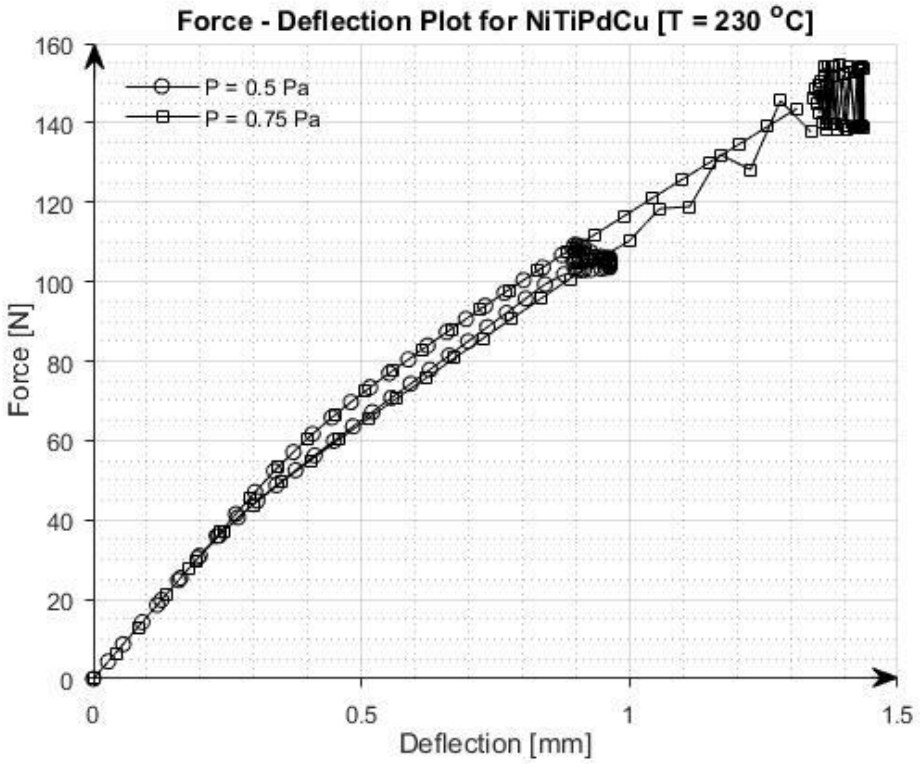

Figure 3.49 Force *vs.* Deflectin for NiTiPdCu at T = 230 °C.

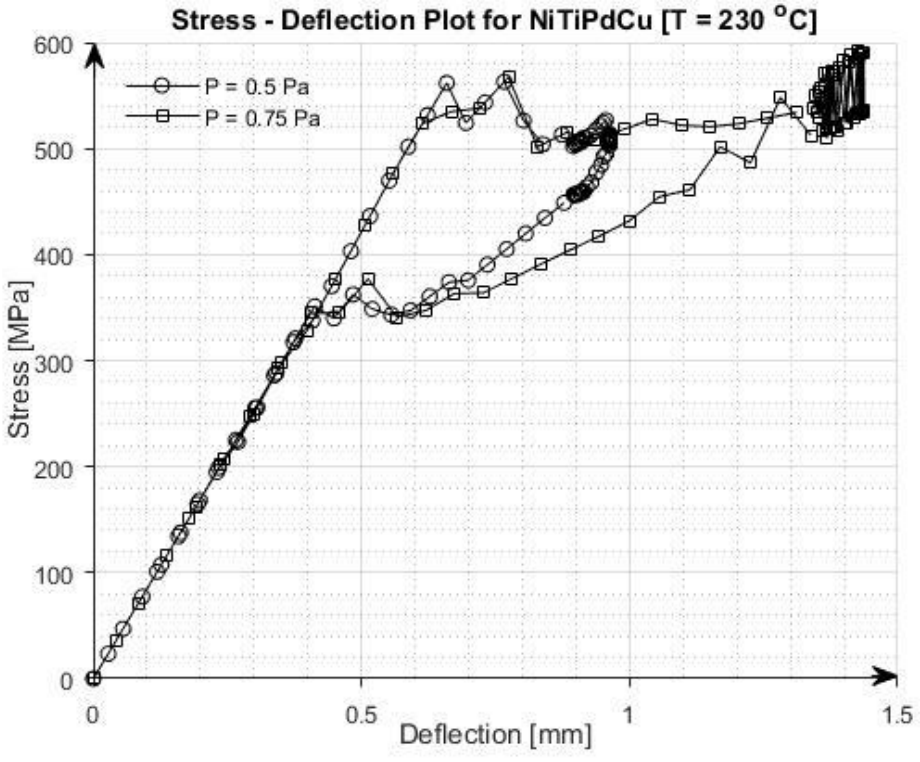

Figure 3.50 Stress *vs.* Deflection for NiTiPdCu at T = 230 °C.

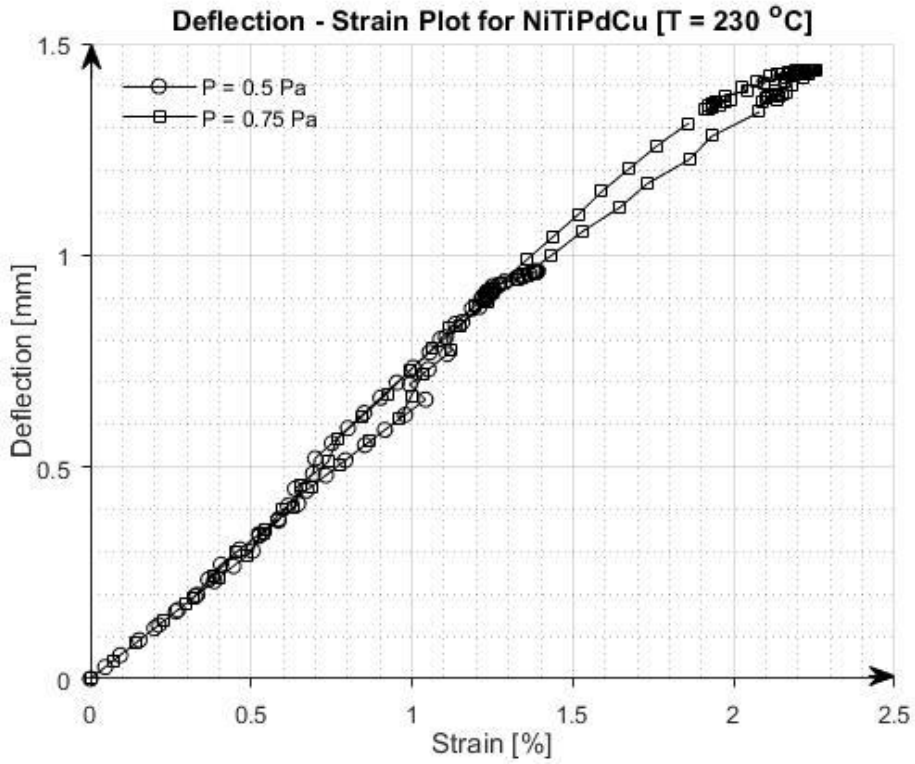

Figure 3.51 Deflection *vs.* Strain for NiTiPdCu at T = 230 °C.

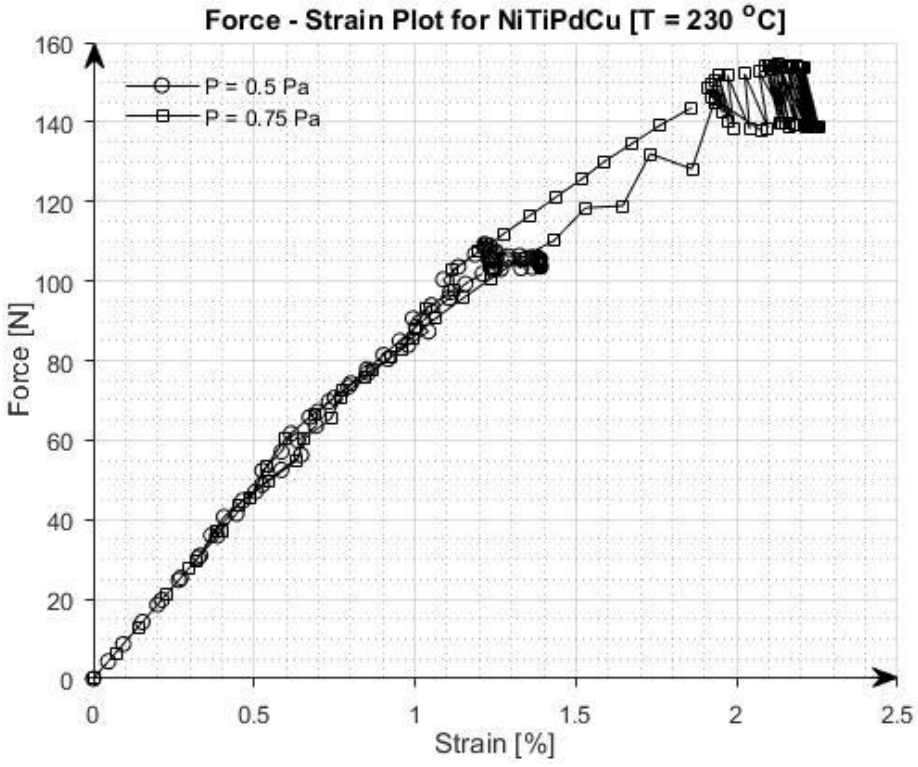

Figure 3.52 Force *vs.* Strain for NiTiPdCu at T = 230 °C.

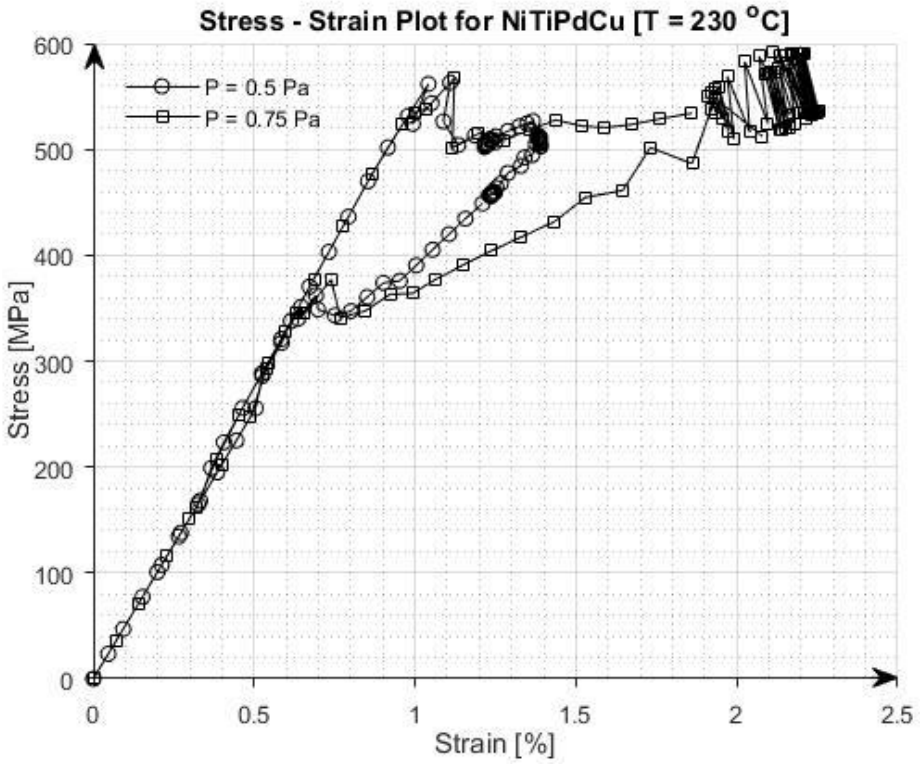

Figure 3.53 Stress *vs.* Strain for NiTiPdCu at T = 230 °C.

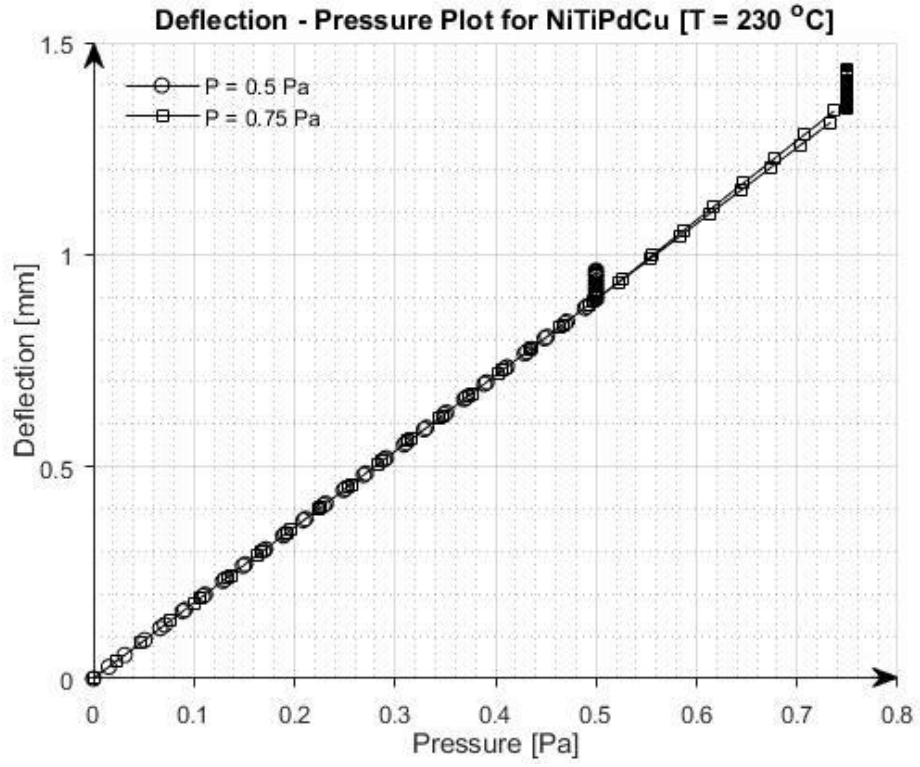

Figure 3.54 Deflection *vs.* Pressure for NiTiPdCu at T = 230 °C.

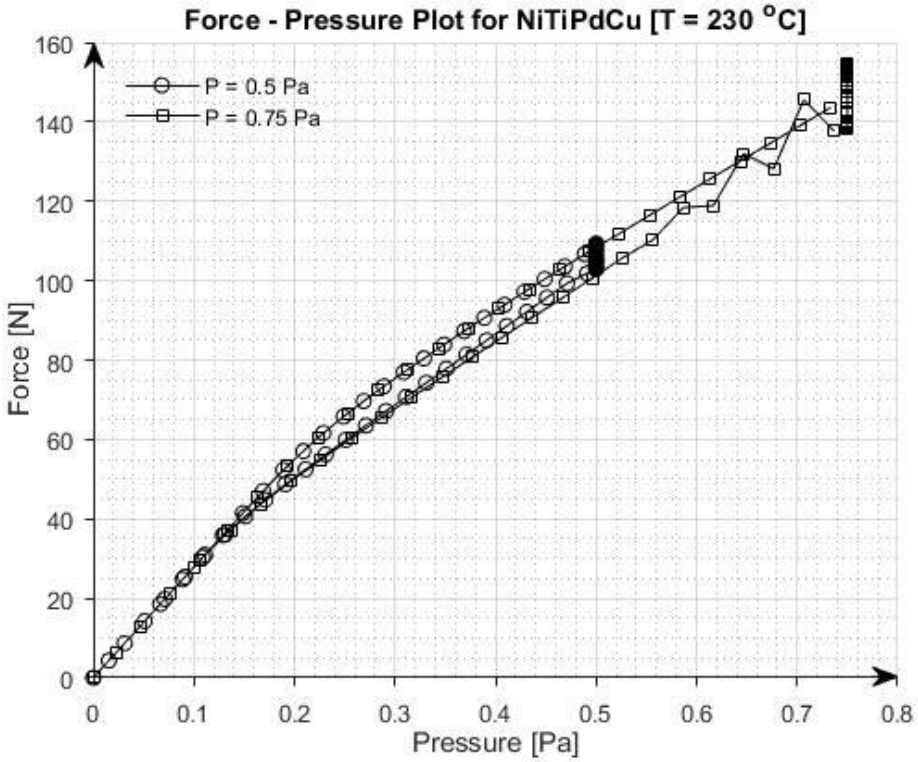

Figure 3.55 Force *vs.* Pressure for NiTiPdCu at T = 230 °C.

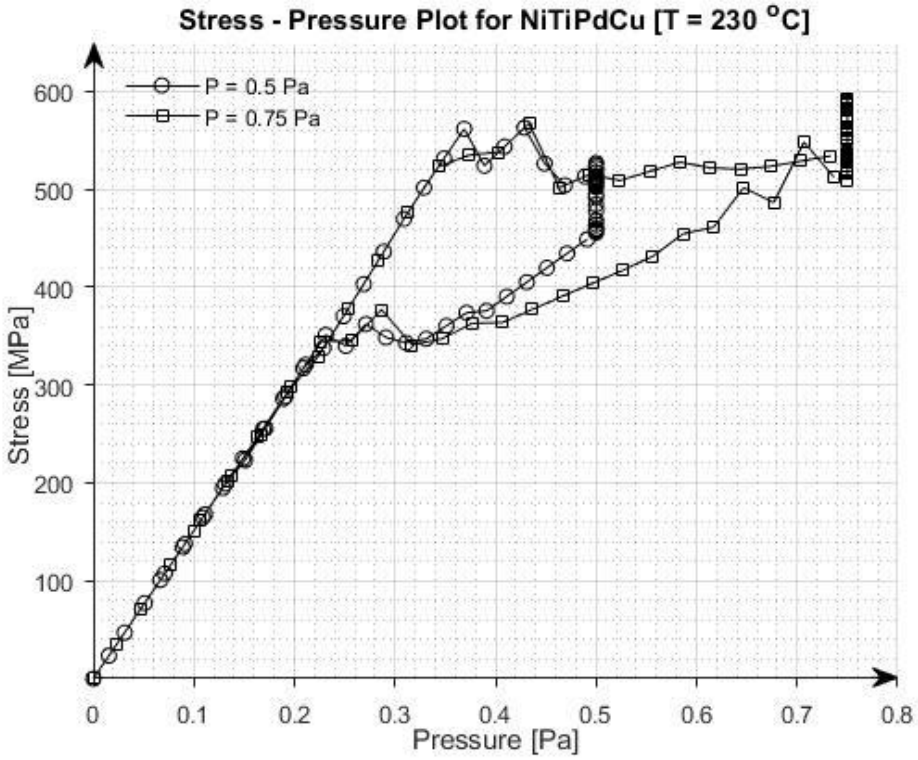

Figure 3.56 Stress *vs.* Pressure for NiTiPdCu at T = 230 °C.

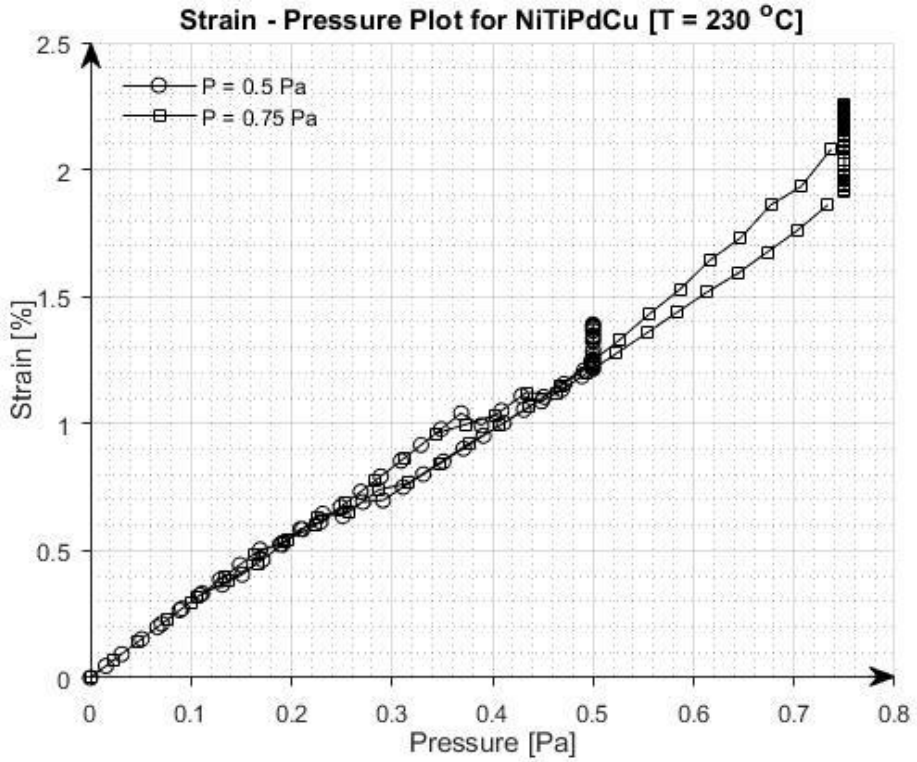

Figure 3.57 Strain *vs.* Pressure for NiTiPdCu at T = 230 °C.

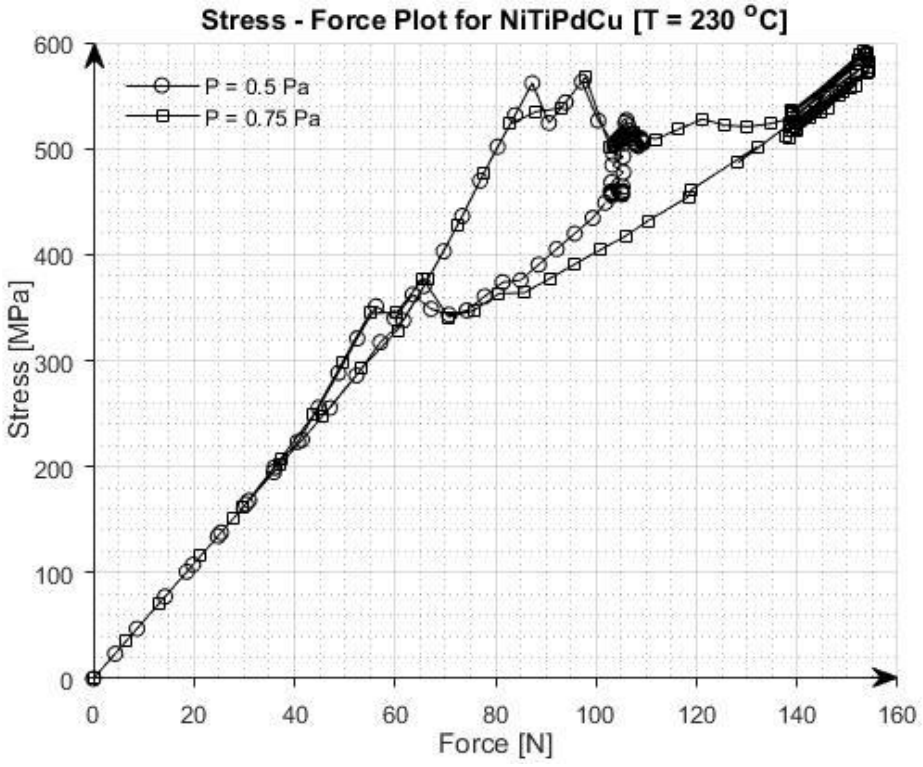

Figure 3.58 Stress *vs.* Force for NiTiPdCu at T = 230 °C.

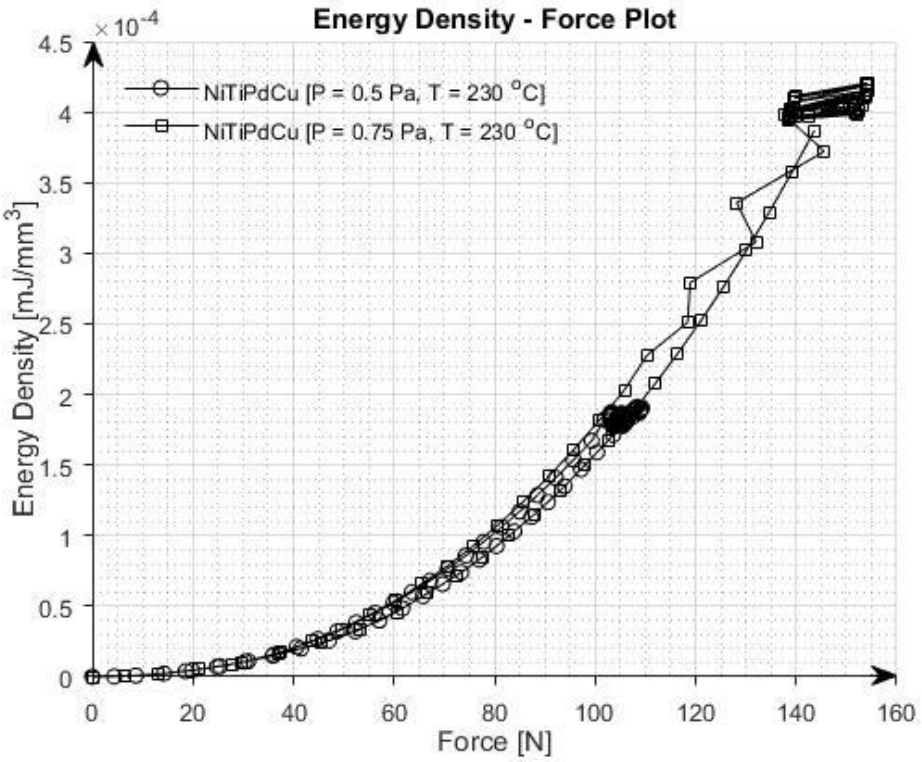

Figure 3.59 Energy density *vs.* Force for NiTiPdCu at T = 230 °C.

CHAPTER 4

RESULTS AND DISCUSSION

The spring is analysed with two smart materials $Ni_{19.5}Ti_{50.5}Pd_{25}Pt_5$ and $Ni_{15}Ti_{50}Pd_{25}Cu_{10}$ at various temperatures and under a range of axial forces. In simulations, the spring is analysed under ±40 N, ±100 N, 125 N, 2000 N force and under 0.50 and 0.75 Pa pressure. All these analyses are run at 250 ºC and 320 ºC. The following parameters are analysed in each simulation:

1. Deflection
2. Stress
3. Strain
4. Energy density

And these parameters are analysed against the following parameters:

1. Temperature
2. Deflection
3. Strain
4. Force

4.1 Results

4.1.1 SMAs under 40 N force

Figure 3.6 represents that both SMAs follows the same path of deflection against temperature plot and also return from the same path. Figure 3.7 represents that the path of both SMAs are different in stress against temperature plot although the both SMAs kept their path for return. The same behaviour is observed in the strain against temperature plot (Figure 3.8). Figure 3.9 represents that NiTiPdCu moved up and returned in the same pattern but NiTiPdPt did not follow the same path for return in energy density against temperature plot. Figure 3.10

represents that both SMAs are very close in following the curve for force against deflection plot though when the spring is compressed, the return path is different.

Figure 3.11 represents the same behaviour with a change that appears in NiTiPdPt which shows too high stress as compare to NiTiPdCu under ±40 N force in stress against deflection plot. Figure 3.12 represents the deflection of NiTiPdCu stopped at 0.6% while that of NiTiPdPt went up to 0.95% though both SMAs return following the same path in deflection against strain plot. Figure 3.14 represents the straight line plot without any sign of transformation of both SMAs under ±40 N force in stress against strain plot. Figure 3.15 represents that the effect of force on spring is minimal i.e. only 40 MPa stress was built up under the force of 39 N in stress against force plot.

4.1.2 SMAs under 100 N force

Figure 3.16 represents the different paths followed by each SMA whereas on return, NiTiPdCu took the same path while NiTiPdPt deviated a bit from its original path in deflection against temperature plot. The same behaviour is observed for the both SMAs in stress against temperature plot (Figure 3.17). Figure 3.18 represents that the deviation is captured at transformation phase only, rest of the curve is same for both ways in strain against temperature plot for both SMAs. The same behaviour is again observed in energy density against temperature plot (Figure 3.19).

Figure 3.20 represents the path followed by both SMAs are same in force deflection plot. Figure 3.21 represents the difference of paths of both SMAs, the stresses reached up to 550 MPa in case of NiTiPdPt while it remained 325 MPa in case of NiTiPdCu in stress deflection plot. Figure 3.22 represents the same abrupt behaviour of path for NiTiPdPt though NiTiPdCu followed the same path in both ways in deflection against deflection plot.

Figure 3.23 represents the residual strain on the removal of force from NiTiPdPt but no such occurrence observed in NiTiPdCu in force against strain plot. Figure 3.24 represents the straight line behaviour without any phase transformation in both SMAs in stress against strain plot. Figure 3.25 represents more inclination of graph of NiTiPdCu than that of NiTiPdPt but the former has less stress than later in stress against force plot.

4.1.3 NiTiPdPt under 125 N force

Figure 3.26 represents the same path followed for both ways for NiTiPdPt in deflection against temperature plot. Figure 3.27 represents the same path followed at the transformation temperature range but the different of path is observed at 25 ºC to 125 ºC temperature in stress against temperature plot. The same behaviour is observed in strain against temperature plot (Figure 3.28). Figure 3.29 represents the same path followed for both ways in transformation phase but it shows deviation at 50 ºC to 160 ºC in energy density against temperature plot.

Figure 3.30 represents the same path followed in both ways while applying force or removal of force in force against deflection plot. Figure 3.31 represents a bit abruptness in the behaviour of both ways but that small deviation can be neglected on the basis of alloying composition in stress against deflection plot. Figure 3.32 represents the effect of residual strain up to 0.1% for NiTiPdPt in deflection against strain plot. The same behaviour is observed in force against strain plot (Figure 3.33). Figure 3.34 represents the same straight line behaviour which followed the same path in both ways in stress against strain plot. Figure 3.35 represents a small amount of residual stresses on the removal of force i.e. about 15 MPa though it followed the same path until on removal of force up to 50 N in stress against force plot.

4.1.4 NiTiPdCu under 2000 N force

Figure 3.36 represents the same path followed behaviour on heating and cooling with a small deflection which reconciles on further cooling even under 2000 N compressive force in stress against temperature plot. The same behaviour is observed in deflection against temperature plot (Figure 3.37). Figure 3.38 represents a lot of energy density with much deviation in energy density against temperature plot. Figure 3.39 represents the typical behaviour of any SMA on application and removal of force and it shows hysteresis loop for NiTiPdCu in force against deflection plot.

Figure 3.40 represents the stress up to 1.8 GPa which returned on the different path but matches before removal of stress in stress against defection plot. Figure 3.41 represents a small deviation of paths on extension and compression but it was removed in the absence of forces in deflection against strain plot. The same graph was observed in force against strain plot (Figure 3.42). Figure 3.43 represents the stress reaches up to 1.8 GPa while strain reaches up to 12% which was not achieved before with NiTiPdPt in stress against strain plot. The same behaviour is seen in stress against force plot (Figure 3.44).

4.1.5 NiTiPdCu under 0.50 Pa and 0.75 Pa pressure

Figure 3.45 represents the deflection up to 0.8 mm and 1.35 mm for NiTiPdCu under pressure of 0.50 Pa and 0.75 Pa respectively in deflection against temperature plot. Figure 3.46 represents the stress of NiTiPdCu reaches up to 500 MPa and 580 MPa under pressure of 0.50 Pa and 0.75 Pa respectively in stress against temperature plot. Figure 3.47 represents the strain up to 1.4% and 2.2% under pressure of 0.50 Pa and 0.75 Pa respectively in strain temperature plot. Figure 3.48 represent notable difference in energy density i.e. 2×10^{-4} mJ/mm^3 and 4.3×10^{-4} mJ/mm^3 under pressure of 0.50 Pa and 0.75 Pa respectively in energy density against temperature plot.

Figure 3.49 represent the force reached up to 110 N and 155 N under pressure of 0.50 Pa and 0.75 Pa respectively in force deflection plot. Figure 3.50 represents much deviated graphs of stress which reconciles on the removal of pressure in stress and deflection plot. Figure 3.51 represents the behaviour is too close under pressure of 0.50 Pa and 0.75 Pa in deflection against strain plot. The same behaviour is observed in the force against strain plot (Figure 3.52). Figure 3.53 represents the straight line behaviour of NiTiPdCu under pressure of 0.50 Pa and 0.75 Pa in deflection against pressure plot. Figure 3.55 represents a small deviation in paths under pressure of 0.50 Pa and 0.75 Pa in force against pressure plot.

Figure 3.56 represents a huge deviation of paths and hysteresis loop under pressure of 0.50 Pa and 0.75 Pa in stress against pressure plot. Figure 3.57 represents very close paths of strains under pressure of 0.50 Pa and 0.75 Pa in strain against pressure plot. Figure 3.58 represent the same abrupt behaviour of stress which later on reconciles on the removal of pressure under 0.50 Pa and 0.75 Pa pressure in stress against deflection plot. Figure 3.59 represents the parabolic relationship of the curve under pressure of 0.50 Pa and 0.75 Pa in energy density against force plot.

4.2 Discussion

The behaviour of stress, strain, deflection and energy density against temperature, force and pressure are presented in the result section which gives very clear comparison of the both SMAs. In each graph plotted above in chapter 3 and as the results presented in this chapter, both SMAs show some advantage on one another but these positive points needs to be analyzed and discussed critically before reaching to a conclusion. The ability to withstand with force

without causing residual stresses in evident in NiTiPdCu while the effect of deflection is less appeared in NiTiPdPt. At some points, the curves of the plots deviated a lot from their original path and this behaviour is portrayed by both SMAs. Another important factor which decides the usability of a material as a spring material is energy density that how much energy can it absorb before failure. The more energy a material can absorb, the better it is considered for spring or actuator application. And also, how much energy is required to cause a change in unit length which can be observed in the form of strain.

CHAPTER 5

CONCLUSION AND FUTURE WORK

The results and discussion favours that the newly composed $Ni_{15}Ti_{50}Pd_{25}Cu_{10}$ alloy is better for spring material than $Ni_{19.5}Ti_{50.5}Pd_{25}Pt_5$ alloy since it has better thermomechanical properties than old one.

The curves and behaviour of numerically simulated NiTiPdCu is same as numerically and experimentally tested NiTiPdPt. This is evident for the soundness of the FEA to predict the behaviour of newly composed SMA rather than directing towards costly and time-consuming long way of experimentations. Before implementation in any FEA package, one must know the constitutive models available in that open-source or commercial FEA package. Unawareness may lead to drastically wrong results.

Since these simulations are run and analysed only under dynamic axial loading but torsional loading is also very crucial in determining the strength, life and fatigue of the spring. It was not the case here as only axial loading was present in the real case scenario hence to reduce computational power, only spring is tested as various temperatures and axial loadings. One future work could be added to simulate the same for torsional loading and later on superposition of both axial and torsional effects can be obtained for those scenarios where both loadings are present.

REFERENCES

[1] D. Culley, S. Garg, S. J. Hiller, W. Horn, A. Kumar, H. K. Mathews, *et al.*, "More Intelligent Gas Turbine Engines," Research and Technology Organisation (RTO), North Atlantic Treaty Organisation (NATO), Neuilly-sur-Seine Cedex, France AC/323(AVT-128)TP/255, 2009.

[2] J. Gore, A. Bowles, M. Maylin, L. Chandrasekaran, D. Forsyth, and M. Buyers, "High Temperature Shape Memory Alloy Actuators through Mechanical Treatments for an Oil & Gas Down-Hole Valve," in *SPIE 6930*, 2008, p. 11.

[3] N. G. Eror, S. N. Coppersmith, P. D. Dean, R. W. Murray, P. S. Peercy, C. A. Rogers, *et al.*, *Expanding the Vision of Sensor Materials*. Washington, D.C., United States of America: National Academy Press, 1995.

[4] Y. Chemisky, G. Chatzigeorgiou, P. Kumar, and D. C. Lagoudas, "A Constitutive Model for Cyclic Actuation of High-Temperature Shape Memory Alloys," *Mechanics of Materials*, vol. 68 no. 2014, pp. 120-136, 2014.

[5] H. J. Maier, "A Focus on High-Temperature Shape Memory Alloys," *Shape Memory Superelasicity*, vol. 2015 p. 1, 2015.

[6] G. S. Shaw, J. T. Snyder, T. S. Prince, and M. C. Willet, "A High Temperature Shape Memory Alloy Sensor for Combustion Monitoring and Control," in *SPIE Vol. 5762*, Bellingham, WA, 2005, pp. 17-26.

[7] V. Miralles, A. Huerre, F. Malloggi, and M.-C. Jullien, "A Review of Heating and Temperature Control in Microfluidic Systems: Techniques and Applications," *Diagnostics*, vol. 3 pp. 33-67, 2013.

[8] C. M. Wayman, "Shape Memory Alloys," *Materials Reseach Society Bulletin*, vol. 18 no. 4, pp. 49-56, 1993.

[9] J. M. Jani, M. Leary, A. Subic, and M. A. Gibson, "A Review of Shape Memory Alloy Research, Applications and Opportunities," *Materials and Design*, vol. 56 pp. 1078–1113, 2014.

[10] T. W. Duerig, K. N. Melton, and D. Stöckel, *Engineering Aspects of Shape Memory Alloys*, 1st ed. Boston: Butterworth-Heinemann, 1990.

[11] Y. Liu, M. Kohl, K. Okutsu, and S. Miyazaki, "A TiNiPd Thin Film Microvalve for High Temperature Applications," *Materials Science and Engineering A*, vol. 378 pp. 205-209, 2004.

[12] A. P. Stebner, "Development, Characterization, and Application of $Ni_{19.5}Ti_{50.5}Pd_{25}Pt_5$ High-Temperature Shape Memory Alloy Helical Actuators," Master of Science M.S, Materials and Metallurgy, University of Akron, USA, 2007.

[13] G. Song, D. Patil, C. Kocurek, and J. Bartos, "Applications of Shape Memory Alloys in Offshore Oil and Gas Industry: A Review," *Earth and Space: Engineering, Science, Construction, and Operations in Challenging Environments,* vol. 2010 pp. 1551-1567, 2010.

[14] S. Padula-II, G. Bigelow, R. Noebe, D. Gaydosh, and A. Garg, "Challenges and Progress in the Development of High-Temperature Shape Memory Alloys Based on NiTiX Compositions for High-Force Actuator Applications," Cleveland, Ohio, United States of America2007.

[15] A. Stebner, S. A. Padul-II, R. D. Noebe, and D. D. Quinn, "Characterization of $Ni_{19.5}Ti_{50.5}Pd_{25}Pt_5$ High-Temperature Shape Memory Alloy Springs and Their Potential Application in Aeronautics," in *SPIE Vol. 6928*, 2008, p. 12.

[16] W. Soboyejo, *Advanced Structural Materials: Properties, Design Optimization and Applications*. Boca Raton, Florida, United States of America: CRC Press, 2007.

[17] A. Pagano, S. Ameduri, V. Cokonaj, A. E. Rnnova, A. Prachaˇ, Z. Zachariadis, *et al.*, "Helicopter Blade Morphing Strategies Aimed at Mitigating Environmental Impact," *Journal of Theoretical and Applied Mechanics,* vol. 49 no. 4, pp. 1233-1259, 2011.

[18] G. S. Firstov, J. V. Humbeeck, and Y. N. Koval, "High Temperature Shape Memory Alloys Problems and Prospects," *Journal of Intelligent Material Systems and Structures,* vol. 17 no. December, pp. 1041-1047, 2006.

[19] J. J. Epps and I. Chopra, "In-Flight Tracking of Helicopter Rotor Blades using Shape Memory Alloy Actuators," *Smart Materials and Structures,* vol. 10 pp. 104-111, 2001.

[20] S. Ogden, "High-Pressure Microfluidics," Doctor of Philosophy Ph.D, Department of Engineering Sciences, Microsystems Technology, Uppsala Universiy, Uppsala, Sweden, 2013.

[21] H. Prahlad and I. Chopra, "Design of a Variable Twist Tiltrotor Blade Using Shape Memory Alloy (SMA) Actuators," in *SPIE*, 2001, p. 14.

[22] K. Singh and I. Chopra, "Design of an Improved Shape Memory Alloy Actuator for Rotor Blade Tracking," in *SPIE*, 2002, p. 23.

[23] T. R. Quackenbush, B. F. Carpenter, A. H. Boschitsch, and P. V. Danilov, "Development and Test of an HTSMA Supersonic Inlet Ramp Actuator," in *SPIE*, 2008, p. 11.

[24] S. Padula-II, R. Noebe, G. Bigelow, D. Culley, M. Stevens, N. Penney, *et al.*, "Development of a HTSMA-Actuated Surge Control Rod for High-Temperature Turbomachinery Applications," *American Institute of Aeronautics and Astronautics,* 2007.

[25] D. K. Kennedy, F. K. Straub, L. M. Schetky, Z. Chaudhry, and R. Roznoy, "Development of an SMA Actuator for In-flight Rotor Blade Tracking," *Journal Of Intelligent Material Systems and Structures,* vol. 15 no. April, p. 14, 2004.

[26] A. Stebner, S. Padula-III, R. Noebe, B. Lerch, and D. Quinn, "Development, Characterization, and Design Considerations of $Ni_{19.5}Ti_{50.5}Pd_{25}Pt_5$ High-temperature Shape Memory Alloy Helical Actuators," *Journal of Intelligent Material Systems and Structures,* vol. 20 no. November, p. 21, 2009.

[27] D. J. Leo, *Engineering Analysis of Smart Material Systems*. Hoboken, New Jersey, United States of America: John Wiley & Sons, Inc., 2007.

[28] J. V. Humbeeck, "Non-medical Applications of Shape Memory Alloys," *Material Science and Engineering: A,* vol. 273 pp. 134-148, 1999.

[29] F. Gandhi and D. Wolons, "Characterization of the Pseudoelastic Damping Behavior of Shape Memory Alloy Wires using Complex Modulus," *Smart Materials and Structures,* PII: S0964-1726(99)98884-5, vol. 8 pp. 49-56, 1999.

[30] P. R. Barrett and P. Cunningham, "Super Elastic Alloy Eyeglass Frame Design Using the ANSYS Workbench Environment," in *2004 International ANSYS Conference*, Pittsburgh, Pennsylvania, United States of America, 2004.

[31] F. T. Calkins and J. H. Mabe, "Shape Memory Alloy Based Morphing Aerostructures," *Journal of Mechanical Design,* vol. 132 no. November, p. 7, 2009.

[32] W. R. Corwin, S. T. Rosinski, and E. v. Walle, Eds., *Small Specimen Test Techniques*. West Conshohocken, Philadelphia, United States of America: American Society for Testing and Materials (ASTM), 1997, p.^pp. Pages.

[33] D. Kardas, W. Rust, A. Polley, and T. Fabian, "Turning Up the Volume," *ANSYS Advantage,* vol. 1 no. 2, pp. s4-s5, 2007.

[34] D. Patil and G. Song, "Shape Memory Alloy Actuated Accumulator for Ultra-Deepwater Oil and Gas Exploration," *Smart Materials and Structures,* 045012, vol. 25 p. 11, 2016.

[35] D. J. Hartl, J. H. Mabe, O. Benafan, A. Coda, B. Conduit, R. Padan, *et al.*, "Standardization of Shape Memory Alloy Test Methods toward Certification of Aerospace Applications," *Smart Materials and Structures,* 082001, vol. 24 p. 6, 2015.

[36] S. u. Rehman, M. Khan, A. N. Khan, L. Ali, S. Zaman, M. Waseem, *et al.*, "Transformation Behavior and Shape Memory Properties of $Ti_{50}Ni_{15}Pd_{25}Cu_{10}$ High Temperature Shape Memory Alloy at Various Aging Temperatures," *Materials Science & Engineering A,* vol. 619 pp. 171-179, 2014.

[37] N. Caldwell and E. Gutmark, "Heat Transfer Model for Blade Twist Actuator System," *Journal of Thermophysics and Heat Transfer,* vol. 21 no. 2, 2007.

[38] S. Garg, K. Schadow, W. Horn, H. Pfoertner, and I. Stiharu, "Sensor and Actuator Needs for More Intelligent Gas Turbine Engines," in *Turbo Expo*, Glasgow, Scotland, United Kingdom, 2010, p. 20.

[39] S. u. Rehman, M. Khan, A. N. Khan, S. H. I. Jaffery, L. Ali, and A. Mubashar, "Improvement in the Mechanical Properties of High Temperature Shape Memory Alloy ($Ti_{50}Ni_{25}Pd_{25}$) by Copper Addition," *Advances in Materials Science and Engineering,* vol. 2015 p. 7, 2015.

[40] S. u. Rehman, M. Khan, L. Ali, and S. H. I. Jaffery, "Effect of aging on Phase Transition Behavior of $Ti_{50}Ni_{15}Pd_{25}Cu_{10}$ HighTemperature Shape Memory Alloys," *Advanced Materials Research,* vol. 1101 pp. 177-180, 2015.

[41] A. International, "Standard Test Method for Tension Testing of Nickel-Titanium Superelastic Materials," vol. F2516 − 14, ed. West Conshohocken, Philadelphia, United States of America: ASTM International, 2015, p. 6.

[42] S. u. Rehman, M. Khan, A. N. Khan, L. Ali, and S. H. I. Jaffery, "Two-Step Martensitic Transformation in an Aged $Ti_{50}Ni_{15}Pd_{25}Cu_{10}$ High Temperature Shape Memory Alloys," *Acta Physica Polonica A,* vol. 128 pp. 125-128, 2015.

[43] T. Quackenbush and J. Robert Mckillip, "Selected Applications of Aeropropulsion Actuation and Shape Control Devices Using HTSMAs," *Metallurgical and Materials Transactions A,* vol. 43A no. August, pp. 2870-2881, 2011.

[44] A. International, "Standard Test Method for Tensile Properties of Single Textile Fibers," vol. D3822/D3822M − 14, ed. West Conshohocken, Philadelphia, United States of America: ASTM International, 2014, p. 10.

[45] M. Kohl, D. Dittmann, E. Quandt, and B. Winzek, "Thin Film Shape Memory Microvalves with Adjustable Operation Temperature," *Sensors and Actuators,* vol. 83 pp. 214-219, 2000.

[46] O. Rios, "Advanced High-temperature Shape-Memory Alloy Development and Thermomechanical Characterization of Platinum and Palladium Modified NiTi Based

SMAs," Master of Science M.S, University of Florida, Florida, United Stated of America, 2006.

[47] F. Auricchio, J. Arghavani, M. Conti, S. Morganti, A. Reali, and U. Stefanelli, "Shape-Memory Alloys: Effective 3D Modeling, Computational Aspects, Analysis of Actuator and Biomedical Devices," p. 4.

[48] D. E. Nicholson, S. A. Padula-II, R. D. Noebe, O. Benafan, and R. Vaidyanathan, "Thermomechanical Behavior of NiTiPdPt High Temperature Shape Memory Alloy Springs," *Smart Materials and Structures*, 125009, vol. 23 p. 13, 2014.

[49] M. Kawakita, M. Takahashi, S. Takahashi, and Y. Yamabe-Mitarai, "Effect of Zr on Phase Transformation and High-Temperature Shape Memory Effect in TiPd Alloys," *Materials Letters*, vol. 89 pp. 336–338, 2012.

[50] J. P. Dunne, M. A. Hopkins, E. W. Baumann, D. M. Pitt, and E. V. White, "Overview of the SAMPSON Smart Inlet," in *SPIE*, Newport Beach, California, United States of America, 1999, p. 11.

[51] R. A. A. d. Aguiar, J. H. I. Pereira, C. G. d. Souza, P. M. C. L. Pacheco, and M. A. Savi, "Shape Memory Alloy Helical Springs: Modeling, Simulation and Experimental Analysis," in *Mechanics of Solids*, Brazil, 2009.

[52] D. E. Nicholson, "Thermomechanical Behavior of High-Temperature Shape Memory Alloy Ni-Ti-Pd-Pt Actuators," Master of Science MS Thesis, Department of Mechanical, Materials and Aerospace Engineering, College of Engineering and Computer Science, Orlando, Florida, Orlando, Florida, United States of America, 2011.

[53] A. V. Pattekar and M. V. Kothare, "Novel Microfluidic Interconnectors for High Temperature and Pressure Applications," *Journal of Micromechanics and Microengineering*, PII: S0960-1317(03)52726-7, vol. 13 pp. 337–345, 2003.

[54] R. Budynas and K. Nisbett, *Shigley's Mechanical Engineering Design*, 10th ed. New York: McGraw-Hill Education, 2014.

[55] S. Imaoka, "Shape Memory Alloy – Superelastic vs. Shape Memory Effect Models," in *International ANSYS Conference*, 2014, p. 10.

[56] J. A. DeCastro, K. J. Melcher, and R. D. Noebe, "System-Level Design of a Shape Memory Alloy Actuator for Active Clearance Control in the High-Pressure Turbine," in *41st Joint Propulsion Conference and Exhibit*, Tucson, Arizona, United States of America, 2015.

[57] S. Marre, J. Baek, J. Park, M. G. Bawendi, and K. F. Jensen, "High-Pressure/HighTemperature Microreactors for Nanostructure Synthesis," *Journal of Association for Laboratory Automation*, vol. 14 no. December, pp. 367-373, 2009.

[58] C. Samónov, "Computer-Aided Design of Helical Compression Spring: Statically Loaded Springs of Round Wire with Residual Stresses induced by Presetting Operation," *ASME*, 80-DET-69, 1980.

[59] A. M. Wahl, *Mechanical Springs*, 2nd ed. New York: McGraw-Hill, 1963.

[60] J. A. Haringx, "On Highly Compressible Helical Springs and Rubber Rods and Their Application for Vibration-Free Mountings," *Philips Res. Rep*, vol. 4 no. February, pp. 49-80, 1949.

[61] J. A. Haringx, "On Highly Compressible Helical Springs and Rubber Rods and Their Application for Vibration-Free Mountings," *Philips Res. Rep*, vol. 3 no. December, pp. 401-449, 1948.

[62] T. Georges, V. Brailovski, and P. Terriault, "Characterization and Design of Antagonistic Shape Memory Alloy Actuators," *Smart Materials and Structures*, 035010, vol. 21 p. 8, 2012.

[63] J. Higgins, "Obtaining and Optimizing Structural Analysis Convergence," in *International ANSYS Conference*, 2012, p. 89.

[64] A. R. A. Paternoster, "Smart Actuation Mechanisms for Helicopter Blades," Doctor of Philosophy PhD Dissertation, University of Twente, Enschede, The Netherlands, 2013.

[65] S. Garg, "NASA Glenn Research in Controls and Diagnostics for Intelligent Aerospace Propulsion Systems," presented at the 17th International Symposium on Airbreathing Engines (ISABE), Munich, Germany, 2005.

Proposed Certificate for Plagiarism

It is certified that MS Thesis Titled **"FEA Validation of NiTiPdPt ans NiTiPdCu Shape Memory Alloys at High Temperatures"** by **Aiman Rashid** has been examined by us. We undertake the follows:

a. Thesis has significant new work/knowledge as compared already published or are under consideration to be published elsewhere. No sentence, equation, diagram, table, paragraph or section has been copied verbatim from previous work unless it is placed under quotation marks and duly referenced.

b. The work presented is original and own work of the author (i.e. there is no plagiarism). No ideas, processes, results or words of others have been presented as Author own work.

c. There is no fabrication of data or results which have been compiled /analyzed.

d. There is no falsification by manipulating research materials, equipment or processes, or changing or omitting data or results such that the research is not accurately represented in the research record.

e. The thesis has been checked using TURNITIN (copy of originality report attached) and found within limits as per HEC plagiarism Policy and instructions issued from time to time.

Name & Signature of Supervisor

Name: **Dr. Mushtaq Khan**

Signature: _____

Originality Report

FEA Validation of NiTiPdPt and NiTiPdCu Shape Memory Alloys at High Temperatures

ORIGINALITY REPORT

%11	%8	%4	%7
SIMILARITY INDEX	INTERNET SOURCES	PUBLICATIONS	STUDENT PAPERS

PRIMARY SOURCES

1	Submitted to Higher Education Commission Pakistan Student Paper	%3
2	www.swedishryk.edu.pk Internet Source	%1
3	www.coursehero.com Internet Source	%1
4	www.macs.hw.ac.uk Internet Source	%1
5	McKeen, Laurence W.. "Polyether Plastics", Effect of Temperature and Other Factors on Plastics and Elastomers, 2014. Publication	%1
6	docslide.us Internet Source	%1
7	en.wikipedia.org Internet Source	<%1

Noebe, Ronald, Tiffany Biles, and Santo

8	Padula. "NiTi-Based High-Temperature Shape-Memory Alloys : Properties, Prospects, and Potential Applications", Materials Engineering, 2006. Publication	<%1
9	Wayman, C.M.. "Shape Memory Alloys", MRS Bulletin, 1993. Publication	<%1
10	Ishida, Akira, and Valery Martynov. "Sputter-Deposited Shape-Memory Alloy Thin Films: Properties and Applications", MRS Bulletin, 2002. Publication	<%1
11	fr.scribd.com Internet Source	<%1
12	"Polyether Plastics", Effect of Temperature and other Factors on Plastics and Elastomers, 2008 Publication	<%1
13	www.docstoc.com Internet Source	<%1
14	D MARGHITU. "Machine Components", Mechanical Engineer s Handbook, 2001 Publication	<%1
15	Submitted to University of Leeds Student Paper	<%1

Benafan, O., A. Garg, R.D. Noebe, G.S.

16	Bigelow, S.A. Padula, D.J. Gaydosh, R. Vaidyanathan, B. Clausen, and S.C. Vogel. "Thermomechanical behavior and microstructural evolution of a Ni(Pd)-rich Ni24.3Ti49.7Pd26 high temperature shape memory alloy", Journal of Alloys and Compounds, 2015. Publication	<%1
17	Submitted to University of Nottingham Student Paper	<%1
18	Submitted to University of Birmingham Student Paper	<%1
19	documents.mx Internet Source	<%1
20	Submitted to University of Melbourne Student Paper	<%1
21	Submitted to University of New South Wales Student Paper	<%1
22	mitwpl.mit.edu Internet Source	<%1
23	Submitted to Middle East Technical University Student Paper	<%1
24	shareok.org Internet Source	<%1

etds.lib.ncku.edu.tw

25	Internet Source	<%1
26	dspace.lib.cranfield.ac.uk Internet Source	<%1
27	Chowdhury, Piyas, and Huseyin Sehitoglu. "A revisit to atomistic rationale for slip in shape memory alloys", Progress in Materials Science, 2017. Publication	<%1
28	Lobel, R.. "Combinatorial fabrication and high-throughput characterization of a Ti-Ni-Cu shape memory thin film composition spread", Materials Science & Engineering A, 20080525 Publication	<%1
29	www.nwd-wc.usace.army.mil Internet Source	<%1
30	pubs.sciepub.com Internet Source	<%1
31	www.answers.com Internet Source	<%1
32	Han, H.P.. "Buckling enhancement of epoxy columns using embedded shape memory alloy spring actuators", Composite Structures, 200602 Publication	<%1

EXCLUDE QUOTES	OFF	EXCLUDE MATCHES	OFF
EXCLUDE BIBLIOGRAPHY	ON		